



Osmotic Forces and Gap Junctions in Spreading Depression: A Computational Model

BRUCE E. SHAPIRO

*Machine Learning Systems Group, Jet Propulsion Laboratory, California Institute of Technology,
4800 Oak Grove Drive, Pasadena, CA 91109*

bshapiro@jpl.nasa.gov

Received ; Revised August 9, 2000; Accepted September 11, 2000

Action Editor: John Huguenard

Abstract. In a computational model of spreading depression (SD), ionic movement through a neuronal syncytium of cells connected by gap junctions is described electrodiffusively. Simulations predict that SD will not occur unless cells are allowed to expand in response to osmotic pressure gradients and K^+ is allowed to move through gap junctions. SD waves of $[K^+]_{out} \approx 25$ to ≈ 60 mM moving at ≈ 2 to ≈ 18 mm/min are predicted over the range of parametric values reported in gray matter, with extracellular space decreasing up to $\approx 50\%$. Predicted waveform shape is qualitatively similar to laboratory reports. The delayed-rectifier, NMDA, BK, and Na^+ currents are predicted to facilitate SD, while SK and A-type K^+ currents and glial activity impede SD. These predictions are consonant with recent findings that gap junction poisons block SD and support the theories that cytosolic diffusion via gap junctions and osmotic forces are important mechanisms underlying SD.

Keywords: spreading depression, neuronal volume, osmosis, gap junctions, potassium

1. Introduction

Spreading depression (SD) (Leão, 1944a, 1944b, 1944c) has been associated with ischemia and epilepsy, may be involved in the etiology of migraine with aura, transient global amnesia (TGA), and concussion and may even confer some protection against subsequent neural injury. It consists of a slowly moving (≈ 2 to ≈ 12 mm/minute) depression of EEG activity, is typically accompanied by a wave of increased blood flow, and is followed by a prolonged period of vasodilation. When observed at a fixed point, a negative shift in the DC surface potential (≈ 5 to ≈ 15 mV, ≈ 30 sec) is followed by a smaller but longer positive voltage shift. At the cellular level, this slow potential change (SPC) coincides with a period of membrane depolarization followed by a longer period of hyperpolarization. Sometimes a brief hyperpolarization also precedes the

SPC. Voltage spikes both precede and follow the wave but disappear during the SPC (Herreras and Somjen, 1993; Herreras et al., 1994). The SPC is accompanied by an interstitial volume reduction of $\approx 25\%$ to $\approx 50\%$, while $[K^+]_{out}$ typically increases to ≈ 40 to ≈ 50 mM, $[Na^+]_{out}$ and $[Cl^-]_{out}$ typically decrease to ≈ 40 to ≈ 60 mM, and $[Ca^{++}]_{out}$ typically decreases to less than 5% of its resting value (Kraig and Nicholson, 1978; Jing et al., 1994). It appears that SD can propagate in any type of gray matter and has been observed in insects, birds, fish, amphibians, and various mammals including humans (Bures et al., 1974). Following wave passage there is usually complete recovery with no lasting damage.

Recent experiments have suggested that gap junctions may be required for the propagation of spreading depression (Martins-Ferreira and Ribeiro, 1995; Nedergaard et al., 1995; Largo et al., 1996). It had

been previously hypothesized that neuroglia, which are widely connected by gap junctions, might play this facilitatory role (Gardner-Medwin, 1981). However, glial poisons do not prevent spreading depression, and SD waves propagate faster when glial cells are poisoned (Largo et al., 1996, 1997a, 1997b). Thus glial cells may hinder rather than facilitate SD. An alternative hypothesis is that the gap junctions are neuronal. It has been theorized that cellular water entry during the early stages of spreading depression may open stretch-gated gap junctions between neurons (Somjen et al., 1992).

A novel model of spreading depression is presented, which differs from previous biophysical models (Bures et al., 1974; Tuckwell and Miura, 1978; Tuckwell, 1980, 1981; Tuckwell and Hermansen, 1981; Reggia and Montgomery, 1996; Revett et al., 1998) in that it incorporates the effects of gap junctions, cytosolic voltage gradients, and osmotic volume changes. The earlier models are all based on interstitial K^+ diffusion, do not predict any gap-junctional dependence, and do not relate the characteristics of spreading depression to either cell volume or osmotically induced ion movements. Furthermore, these models do not relate either the waveform shape or speed to specific biophysical substrates (such as the effects of specific ion channels). Finally, the predicted wave speeds are not robust but are limited to a subset of the observed physiological range.

In the new model ions are allowed to move electrodiffusively through a cytosolic continuum of neurons connected by gap junctions. Extracellular diffusional movement is also allowed, but simulations show that this motion is less significant than other components of the model. Osmotic pressure gradients develop as ionic populations redistribute; these are equalized by the flow of water through neuronal membranes. The model predicts that SD propagation is driven by a combination of (1) K^+ movement through interneuronal gap junctions, (2) neuronal K^+ efflux through cytoplasmic membrane channels, and (3) osmotically induced volume changes. The simulations also predict that SD will not occur when either gap junctions or osmotic forces are blocked. Membrane currents (primarily of K^+) affect SD wave propagation combinatorially, with waveform properties depending on the specific combination of ionic conductances present in the tissue or organ being studied. Other ions contribute to SD, but their effect is less significant than K^+ . Since the actual combination of ion channels present varies between different brain regions, the simulations

suggest that the properties of SD should also vary between these regions.

2. Methods

2.1. Continuum Model

Cortical tissue is described as a one-dimensional continuum with two compartments representing cytosolic and interstitial space. The cytosolic compartment represents a syncytium of neurons connected by gap junctions, and the interstitial compartment represents the fluid-filled region between cells in the neuropil. The space occupied by non-neuronal cells is not modeled, although glial activity that normally maintains extracellular homeostasis is included. The x axis may be loosely interpreted as a path along the cortical surface. However, the model is completely compatible with a reinterpretation of the x axis as being oblique to the cortical surface, so long as the fixed (constant) parameter values (such as the concentration of each ion channel) are replaced with a spatially varying distribution. This would explain why the properties of the SD response are strongly dependent on depth. Variation in the characteristics of spreading depression with distance (or depth) can thus be attributed to a variation in the parameter values (such as distribution of ionic conductances) with position.

To make the problem computationally tractable, the specific neuronal geometry and connectivity are not considered. Since this is a continuum model, the concept of individual cells is not meaningful. Cellular properties refer to the average values at any location within gray-matter tissue (for a further discussion of the continuum interpretation, see Tuckwell and Miura, 1978). All parameters are taken to range over known dendritic and somatic values. For discussion purposes only, gray matter is referred to as *dendritic* to explicitly distinguish it from white matter, although it should be clear that this tissue contains both cell bodies (somata) and axonal endings and that SD occurs in both somata and dendrites.

The model system has 29 state variables: the cytosolic and interstitial concentrations of K^+ , Na^+ , Cl^- , and Ca^{++} ; the neuronal volume fraction f ; the cytosolic IP3 (1,4,5-inositol trisphosphate) concentration; the buffered Ca^{++} concentration; and 18 Hodgkin-Huxley variables. The cytosolic concentration c_{in} of each ion (K^+ , Na^+ , Cl^- , and Ca^{++}) is described by a separate

electrodiffusion equation (Qian and Sejnowski, 1989):

$$\frac{\partial c_{in}}{\partial t} = \frac{\partial}{\partial x} \left(D_{c,in} \frac{\partial c_{in}}{\partial x} \right) + \frac{zF}{RT} \frac{\partial}{\partial x} \left(c_{in} D_{c,in} \frac{\partial V}{\partial x} \right) - \kappa J_{c,m} + s_c, \quad (1)$$

where $D_{c,in}$ is the cytosolic diffusion constant of c , z is the valence, V is the membrane potential, T is the temperature, $F \approx 96$ coul/mM is Faraday's constant, $R \approx 8.314$ J/mole-Kelvin is the ideal gas constant, κ is the average dendritic surface area to volume ratio ($\kappa = 4/d$ for a cylindrical process of diameter d), $J_{c,m}$ is the membrane flux of species c , including ion pumps, and s_c gives the intercellular production (sources) of c (Ca^{++} only). The voltage is calculated using a Goldman-Hodgkin-Katz voltage equation. The movement of ions through gap junctions is described by interpreting $D_{c,in}$ as the effective diffusion constant through the cytosolic continuum rather than the diffusion constant within a single cell (Keener and Sneyd, 1998).

Currents predicted by Eq. (1) are nearly identical to those obtained in the more traditional compartmental approximations to the cable equation under normal physiological condition—that is, when the concentration changes are small with respect to their resting values (Qian and Sejnowski, 1989). The assumption of small concentration changes is not valid during spreading depression, however, when there are large ionic fluxes, and it is therefore necessary to include the electrodiffusive term in Eq. (1) (the second term on the right-hand side of Eq. (1)).

The original derivation assumes cylindrical symmetry (Qian and Sejnowski, 1989), but it is possible to derive Eq. (1) under less stringent restrictions that allow for spines and variations in dendritic radius (Shapiro, 2000). However, this generalization still requires a cylindrical or longitudinal geometry and is not appropriate for somatic geometry. The surface area of cortical dendrites has been estimated at one to two orders of magnitude larger than the surface area of somata (Douglas and Martin, 1998). Hence it would seem reasonable, within the scope of a continuum model, to treat gray matter as principally dendritic. In fact, it is not at all clear how to generalize Eq. (1) to incorporate more general geometry. Thus geometric parameters have been used that correspond to dendrites (radii ≈ 0.2 to $10 \mu\text{M}$). With this one exception, all other parameters in the model have been chosen to range over

the entire range of observed gray-matter values, both dendritic and somatic.

The corresponding interstitial ionic concentrations are described by standard reaction-diffusion equations of the form

$$\frac{\partial c_{out}}{\partial t} = D_{c,out} \frac{\partial^2 c_{out}}{\partial x^2} + \frac{\kappa f}{1-f} J_{c,m} - J_{c,glia} \quad (2)$$

for each species, where $D_{c,out}$ is the interstitial diffusion constant of c and $J_{c,glia}$ describes glial uptake.

2.2. Gap Junctions

A number of lines of research suggest the presence of neuronal gap junctions. Recent experiments have suggested that connexin proteins are widely distributed in the human brain (Belluardo et al., 1999), and interneuronal dye coupling has been observed in the rat brain (Peinado et al., 1993). Clusters of gap junctions have been identified throughout the length of rat spinal motoneuron dendrites with electron microscopy; most intracellular organelles (ER and mitochondria) appear to absent from the immediate vicinity of these junctions, although the biophysical significance of this observation is not clear (van der Want et al., 1998). Very little is known about the localization of gap junctions within neurons. Studies of stellate cells in the sensory and motor cortex of the adult rhesus monkey (*macaca mulatta*) indicate that gap junctions are primarily dendrodendritic (76% of $n = 25$), with smaller quantities being dendrosomatic (16%) and dendro-dendritic-spine (8%) (Sloper and Powell, 1978). This is in contrast to goldfish Mauthner cells, in which large numbers of gap junctions appear to be clustered at synapses (Tuttle et al., 1986). More recently, there has been some indication of widespread gap-junction coupling between neurons and astrocytes in rat brain cultures (Fróes et al., 1999; Nadarajah and Parnavelas, 1999).

Since the gating properties of neuronal gap junctions have not been characterized in any detail, the movement of ions through gap junctions is described with an ad hoc diffusional model. In this approach, $D_{c,in}$ in Eq. (1) is interpreted as the effective diffusion constant through the cytosolic continuum, modified in a spatially and electrotonically dependent fashion to reflect the purported properties of gap junctions (as described in the following paragraph). A full description of spreading depression will need to describe complete network connectivity including gap-junction

gating models. Such an approach is probably unrealistic at the present time, however, because the large distances (on the order of several millimeters) that must be described to model wave propagation. The diffusional/continuum approach significantly reduces the computational demands on the model.

In cardiac cells there is some indication of voltage, Ca^{++} , and pH dependent gating. Gap junctions between rat atrial myocytes close with a half-inactivation voltage of ≈ 40 to ≈ 50 mV between adjacent cells (Boltzmann distribution fit) (Lal and Arnsdorf, 1992). Vogel and Weingart (1998) suggest that the half-inactivation voltage ranges from ≈ 50 to ≈ 1000 mV. Noma and Tsuboi estimate Hill constants for H^+ inactivation of ≈ 2.3 and for Ca^{++} of ≈ 3.4 , and half-inactivation $\text{pH} \approx -6.95$ and $\text{pCa} \approx -6.50$ ($[\text{Ca}^{++}]_{1/2} = 316$ nM) in guinea pig cardiac cells (Noma and Tsuboi, 1987). There have been no reports (or models) of membrane stretch affecting neuronal gap junctions. Gap-junction inactivation is described by expressing the cytoplasmic diffusion constant in Eq. (1) as

$$D_{c,in} = D_0 \gamma(\Delta V) B([\text{H}^+], [\text{Ca}^{++}]). \quad (3)$$

Here $\gamma(\Delta V)$ describes the voltage dependence, where ΔV is the voltage drop across the junction, and $B([\text{H}^+], [\text{Ca}^{++}])$ describes ionic block due to protons and calcium. The voltage dependence is described by the model of Vogel and Weingart (1998) and ionic block by the model of Noma and Tsuboi (1987). The specific equations for γ and B are given in the appendix.

2.3. Osmotic Forces

Assuming the system is initially neutral, the total number N_A of cytosolic impermeant anions in a volume element \mathcal{V} (cytosolic plus interstitial) is

$$N_A = \mathcal{V}_{rest}([\text{Na}^+]_{in,rest} + [\text{K}^+]_{in,rest} - [\text{Cl}^-]_{in,rest}). \quad (4)$$

Since these anions are membrane-impermeant (including via gap junctions), the value of N_A is fixed. Furthermore, in isotonic balance, the internal and external solute concentrations should be equal. Under this assumption the total interstitial solute concentration

$[\text{S}]_{out}$ is

$$[\text{S}]_{out} = [\text{Na}^+]_{in} + [\text{K}^+]_{in} + [\text{Cl}^-]_{in} + \frac{N_A}{f\mathcal{V}} \quad (5)$$

at any time. To maintain this isotonicity, any change in the ionic concentration is balanced in the model by a flow of water across the membrane such that $\Delta\mathcal{V}/\mathcal{V} = \Delta N_S/N_S$, where N_S is the total number of interstitial solute ions in the interstitial volume element. Hence (Jakobson, 1980)

$$\frac{df}{dt} = \begin{cases} \frac{1}{[\text{S}]_{out}} \sum \frac{d}{dt}([c]_{in}f), & f \leq f_{max} \\ 0, & f > f_{max}. \end{cases} \quad (6)$$

Neuronal cells resist swelling more than other cells (Aitken et al., 1998a). Thus cells are not allowed to expand beyond the limits imposed by the surrounding parenchyma, typically to no more than 95% of the total volume (that is, $f_{max} = 0.95$).

2.4. Units and Parameter Values

Unless otherwise specified in this article, units in all equations are millimolar (mM/liter) for concentration, micrometers (μm) for distance, seconds (sec) for time, pico-Siemen per square micrometer ($\text{pS}/\mu\text{m}^2$) for conductance, millimoles per square centimeter per second ($\text{mM}/\text{cm}^2\text{-sec}$) for membrane flux, millimeters per minute (mm/min) for wave speed, and micrometers-squared per second ($\mu\text{m}^2/\text{sec}$) for diffusion constants. Parameter values are based on observed dendritic and somatic values (see Table 1) and are given in the appendix.

2.5. Membrane Currents

The model is shown schematically in Fig. 1. The Hodgkin-Huxley formalism (1952) is used to describe ion channels for K^+ , Na^+ , and Ca^{++} . A passive Cl^- flux is calculated to balance the cation flux. Membrane voltage is determined with the Goldman-Hodgkin-Katz equation (Keener and Sneyd, 1998). The detailed equations are given in the appendix.

2.5.1. Voltage-Gated Potassium Channels. The model includes three voltage-gated K^+ currents: the delayed rectifier (DR), the transient K^+ current (A-channel), and the muscarinic K^+ current (M-channel).

Table 1. Reported gray-matter membrane conductances (pS/cm²). Cell types: HP, hippocampal pyramidal; NP, neocortical pyramidal; P, cerebellar Purkinje; BSG, bullfrog sympathetic ganglion.

Channel	Cell	Dendritic	Somatic	Note
A	HP	5–120		a, b, c
	P	2	15	d
	BSG		25	e
M	NP	20		f
	BSG		17	e
	P	0.1–0.4	0.4–1.4	d
DR	NP	15–23	1350	b, c
	P	600–900	6000–9000	d
	BSG		230	e
BK	HP	40–120	200	b
	P	800		d
	BSG		240	e
IK	P	4		d
SK	HP	8	8	b
	BSG		10	e
Ca (Total)	HP	10–90	10	b, g
Ca (HVA)	P	4–4.5		d
Ca (LVA)	P	0.5		d
Na (F)	HP	0–200	1000	a, b, g, h
	NP	40	45–60	i, j
	P	0	75,000	d
	BSG		400	e
Na (P)	P	0	10	d

a. Conductance varies from proximal to distal.

b. Traub et al. (1994).

c. Hoffman et al. (1997).

d. De Schutter and Bower (1994).

e. Yamada et al. (1998).

f. Mainen and Sejnowski (1998).

g. Magee and Johnston (1995a).

h. Magee and Johnston (1995b).

i. Stuart and Sakmann (1994).

j. Colbert and Johnston (1996).

All three channels have been observed in gray matter (Hoffman et al., 1997). The A-channel is a transient rapidly activating and inactivating channel that is selective for K⁺ and is thought to contribute to spike repolarization. The M-channel allows a noninactivating K⁺ current that can be blocked by muscarinic agonists. The delayed rectifier is expressed in various isoforms throughout the nervous system, and it is the principal contributor to postspike repolarization after an action potential. It has slower kinetics than the A-channel and

M-channel. The models of Yamada, Koch, and Adams (1998) for the bullfrog sympathetic ganglion are used to describe all three of these channels.

2.5.2. K(Ca) Channels. At least three classes of calcium-gated potassium channels (K(Ca)) have been identified in neurons (Blatz and Magleby, 1987; Sah, 1996; Vergara et al., 1998). These are classified based on their calcium and voltage sensitivity and pharmacological properties. The large conductance (BK) channel is both voltage- and Ca⁺⁺-dependent, is sensitive to TEA (tetraethylammonium) and CTX (charybdotoxin), and has a single-channel conductance of ≈200 pS to ≈250 pS. Small conductance (SK) channels have single-channel conductances of ≈4 pS to ≈20 pS, are insensitive to both TEA and CTX, and have at least two subtypes: those that are sensitive to apamin and those that are not. Other K(Ca) channels, which have intermediate single channel conductances (IK) ranging from ≈20 pS to ≈120 pS, are sensitive to both CTX and clotrimazole and are both calcium- and voltage-sensitive. In several neuronal preparations the apamin-sensitive and apamin-insensitive slow after-hyperpolarization (sAHP) currents have been associated with the SK channels. In cerebellar Purkinje cells K(Ca) channels have been identified that activate at lower calcium concentrations than the BK channels and are sensitive to both TEA and CTX (Farley and Rudy, 1988; Reinhart et al., 1989; Groul et al., 1991). These may correspond to IK channels, or there may be two subpopulations of BK channels. The BK and SK channels are described by the models of Yamada, Koch, and Adams (1998). IK channels are described by the K2-channel model of De Schutter and Bower (1994).

2.5.3. Calcium Channels. Several subtypes of voltage-gated calcium currents have been observed in the dendrites of hippocampal pyramidal cells, including both low-voltage-activated (LVA) and high-voltage-activated (HVA) currents. Various pharmacological studies have been consistent with the presence of T-type LVA currents and N, L, P, Q, and R-type HVA-currents in these measurements (Traub et al., 1994; Magee and Johnston 1995a, 1995b; Christie et al., 1995; Gillissen and Alzheimer, 1997; Kavalali et al., 1997). These studies suggest that the different classes of Ca⁺⁺ channels have different distributions in the dendritic tree. Calcium-channel activation and inactivation is described the models of De Schutter and

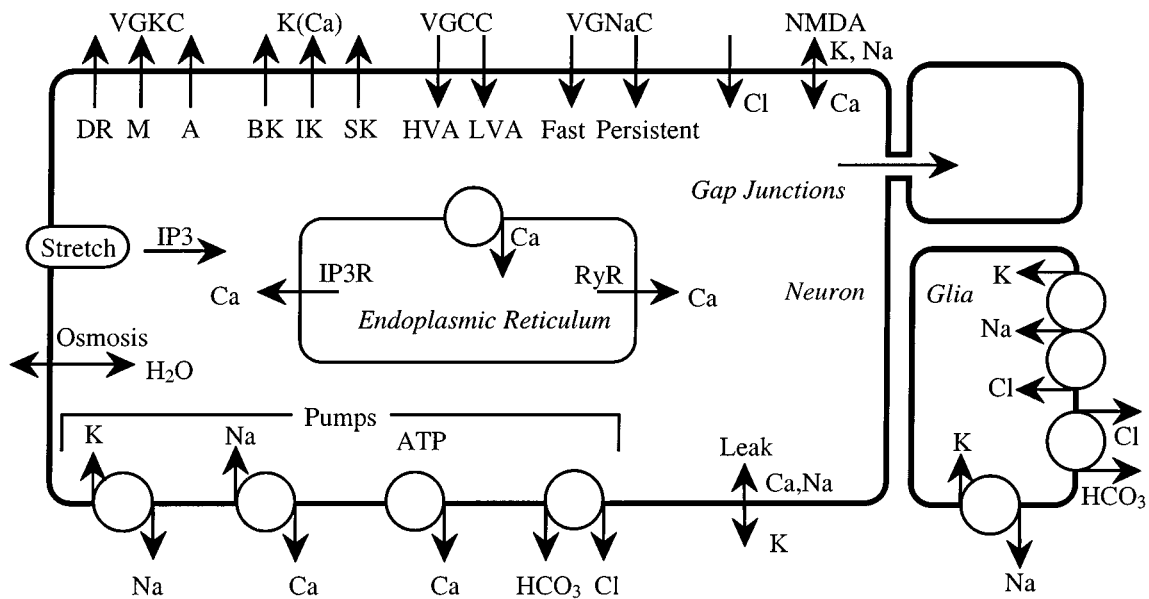


Figure 1. Ionic fluxes included in the model. The membrane has three voltage-gated K^+ currents (VGKC), three Ca^{++} activated K^+ currents ($K(Ca)$), two voltage-gated Ca^{++} currents (VGCC), two voltage-gated Na^+ currents (VGNC), a Cl^- flux, three independently modeled NMDA-activated ion fluxes, and three independent leak currents. There are also four neuronal ion pumps and three glial pumps. Neurons are connected via gap junctions. The endoplasmic reticulum is treated as a large Ca^{++} buffer with IP3 and ryanodine sensitive Ca^{++} channels (IP3R and RyR) and a Ca^{++} pump. IP3 is produced from PIP2 by a stretch-activated process. Water may enter or leave the cell in response to osmotic gradients. Detailed equations for all membrane fluxes are given in the appendix.

Bower (1994). Their T-type and P-type channel models are used as canonical models of the LVA and HVA currents, respectively.

2.5.4. Sodium Channels. In axons, the fast sodium channels is responsible for the large voltage shift that occurs during an action potential. Both fast and persistent Na^+ channels appear to be widely distributed throughout gray matter, although there is some indication that the distribution varies along the length of the dendritic tree (Traub et al., 1994; Stuart and Sakmann, 1994; Magee and Johnston, 1995a, 1995b; Colbert and Johnson, 1996). It may be that the persistent channel is actually a separate gating mode of the fast channel. The models of De Schutter and Bower (1994) are used to describe both of these conductances.

2.5.5. NMDA Channels. The human cerebral cortex contains approximately one synapse per square micron of gray-matter tissue (Koch, 1998). Holmes (1995) estimates that there are 200 to 2,000 NMDA-mediated glutamate receptors in each pyramidal cell synapse. Various measurements indicate that these receptors gate a channel that is permeable to Ca^{++} , K^+ ,

and Na^+ . Furthermore, these currents can be accurately described by independent constant field (Goldman) models—that is, there are no interactions between the different ionic currents (Mayer and Westbrook, 1987; Garaschuk et al., 1996; Schneggenburger, 1996). The current is described as

$$j_{NMDA} = A([Glu], V)B([Mg^{++}], V)j_G, \quad (7)$$

where $A([Glu], V)$ is the neurotransmitter and voltage-dependent activation function (fraction of the channels that are open in the absence of block), $B([Mg^{++}], V)$ describes voltage-dependent Mg^{++} block, and j_G is the Goldman-current through an open pore. The models of Destexhe, Mainen, and Sejnowski (1998) are used to describe channel activation and Mg^{++} block functions (see appendix for detailed equations).

2.5.6. Pumps and Transporters. Because of the lack of specific neuronal models for ion pumps, cardiac models have been used with the pump strengths set to fit neuronal data. K^+ and Na^+ concentrations are maintained by an electrogenic Na^+ , K^+ pump in the cell membrane that pumps three Na^+ ions out of the cell for

every two K^+ ions pumped into the cell. The analytic model given by Lemieux, Roberge, and Joly (1992) for a cardiac pump is used to describe this current. The Ca^{++} gradient is maintained by a high-affinity low-strength membrane-bound ATP-dependent Ca^{++} pump (ATP-ase) and a lower-affinity but higher-strength Na^+ , Ca^{++} exchanger. The Na^+ , Ca^{++} exchanger removes one Ca^{++} ion for every three Na^+ ions pumped in and is described by the cardiac model of Di Francesco and Noble (1985). The ATP-dependent Ca^{++} pump is described by a Michaelis-Menten function with a Hill constant of 1 and a half activation of 200 nM (Di Polo and Beaugé, 1979; De Schutter and Smolen, 1998). Interstitial Na^+ and K^+ balance is maintained by a glial Na^+ , K^+ pump and a Cl^- , Na^+ , K^+ cotransporter that drives all three atoms into glia in the ratio of 2 : 1 : 1. The cotransporter model used is dependent on interstitial K^+ , Na^+ , and Cl^- with Hill coefficient of 1, 1, and 2 and is half-activated at $[K^+]_{out} = 2.7$ mM, $[Na^+]_{out} = 35$ mM and $[Cl^-]_{out} = 40$ mM (Tas et al., 1986; Tas et al., 1987). Cl^- balance is also maintained by a neuronal bicarbonate/ Cl^- exchanger that is modeled with a Hill constant of 1 and that is half-activated at $[Cl^-]_{in} \approx 4$ mM.

2.5.7. Calcium Buffering. The endoplasmic reticulum (ER) has been observed throughout dendritic branches, and the presence of both Ca^{++} -activated ryanodine receptors (RyR) and 1,4,5-inositol trisphosphate (IP3) activated Ca^{++} channels (IP3R) have been established (Berridge, 1993; Kostyuk and Verkhasky, 1995). Buffering into the ER occurs via an ER-membrane-bound Ca^{++} pump. The RyR is described by the reduced quasi-steady-state model suggested by Keener and Sneyd (1998, p. 183). The IP3R and the ER-membrane-bound Ca^{++} pump are described by the models of Atri (Atri et al., 1993; Atri, 1996). Membrane stretch has been observed to induce IP3 production in airway epithelial cells, with the cytosolic IP3 concentration tripling in response to an increase in surface area of $\approx 14\%$ (Felix et al., 1996). While this mechanism has not been reported in neurons, it is hypothesized to exist. A model fit to the data of Felix, Woodruff, and Dirksen (1996) is used to describe IP3 production. IP3 is degraded according to the model of Keener and Sneyd (1998).

2.5.8. Stretch Activation of Ion Channels. Stretch activated ion currents have been observed in a large number of physiological systems. Many voltage-

sensitive K^+ channels—especially the delayed rectifier (Fan and Walsh, 1999; Sasaki et al., 1992), M-channel (Pleumsamran and Kim, 1995; Ji et al., 1998), and BK-type K(Ca) channel (Mienville et al., 1996)—can also be activated by membrane stretch. Stretch activation of several other types of ligand- and voltage-gated currents has also been reported. The probability of channel opening is sigmoidal, increasing with negative pressure (that is, less pressure on the outside of the cell than on the inside of the cell). This probability is described by a Boltzmann distribution.

2.5.9. Glial Cells. Instead of describing the detailed glial kinetics, the glial uptake model is designed to maintain homeostasis against small variations of the interstitial environment. K^+ and Na^+ levels are maintained with both the Na^+ , K^+ exchanger and the Na^+ , K^+ , Cl^- co-transporter. To maintain Cl^- homeostasis a Cl^- , bicarbonate pump is also included. Because of the lack of accurate measurements of the relative pump concentrations in glial cells, the pump strengths are set to give each pump an equal role at steady state. The strength of all glial pumps is then controlled proportionally by a single maximum glial uptake rate r_G for K^+ ($=2$ mM/liter-sec unless otherwise specified). Since the purpose of the present study is to evaluate a model of spreading depression that does not require the presence of glia, glial swelling is not included in the model.

2.6. Implementation

Equations (1) and (2) are integrated for each species using a standard Crank-Nicholson method. The detailed equations are given in the appendix. All models were implemented as FORTRAN computer programs (version 6.0, Absoft Corporation, Rochester Hills, MI) and were run on an Apple iMac (Apple Computer, Inc., Cupertino, CA).

3. Results

3.1. Wave Properties are Independent of Stimulus

The initial stimulation was modeled by raising the interstitial concentration of potassium at $x=0$ to 50 mM/liter with a bell-shaped (Gaussian) distribution ($\sigma = 100 \mu\text{m}$). Other initial concentrations were tested (stimulus ranging from 3 mM to 0.5 M; results not

shown). The model shows a robust threshold in $[K^+]_{out}$, typically at ≈ 20 mM, but with an exact magnitude that depends on the particular combination of ion channels assumed to be present in the tissue. Above threshold, waves propagated and waveform shape, magnitude, and wave speed do not depend on stimulus intensity. Below threshold, waves could not be induced. All of the results presented in this article are based on a stimulus of $[K^+]_{out} = 50$ mM. Repetitive waves are emitted in response to a sustained supra-threshold stimulation (results not shown), although the characteristics of the response to sustained stimuli were not studied in detail.

3.2. Cytosolic K^+ Pulse Precedes DC-Voltage Shift

The predicted DC-voltage shift and ionic concentration changes observed at a fixed point one mm from the stimulation are plotted as a function of time in Fig. 2. In this particular simulation the SD wave begins with a slow increase in $[K^+]_{out}$ to ≈ 10 to ≈ 15 mM that is followed by rapid rise to a peak concentration of ≈ 37 mM. Peak $[K^+]_{out}$ varied from ≈ 25 mM to ≈ 60 mM in other simulations, depending on the particular set of membrane conductances used. During the subsequent ≈ 5 seconds, $[K^+]_{out}$ typically drops by ≈ 5 to ≈ 10 mM to the top of a gently downward-sloping plateau. Over the next ≈ 20 to ≈ 60 seconds, $[K^+]_{out}$ remains on the plateau, dropping by only ≈ 2 to ≈ 5 mM. At the end of this period, $[K^+]_{out}$ rapidly drops to nearly resting levels in ≈ 5 sec. At the same time as the rapid increase in $[K^+]_{out}$ there is a nearly complete disappearance of $[Ca^{++}]_{out}$ and a substantial reduction in $[Na^+]_{out}$ and $[Cl^-]_{out}$ (Cl^- is not shown in Fig. 3 but its predicted behavior is similar to that of Na^+). The minimum concentrations of $[Na^+]_{out}$ and $[Cl^-]_{out}$ are typically ≈ 10 to ≈ 20 mM and of $[Ca^{++}]_{out}$ is ≈ 30 μM ($\approx 1.5\%$ of the resting concentration). These minima occur simultaneously as the maximum of $[K^+]_{out}$. The DC-voltage shift occurs at the same time and has the same qualitative shape as the change in $[K^+]_{out}$. The final rapid decrease of $[K^+]_{out}$ occurs when the plateau in V has decreased to ≈ -50 mV. However, rather than returning to the resting value, V continues to decline for another ≈ 10 mV before leveling off and remains in this hyperpolarized state for a least another minute. The hyperpolarization occurs because the $[Na^+]_{out}$ and $[Cl^-]_{out}$ return to their resting levels more slowly than $[K^+]_{out}$. $[Ca^{++}]_{out}$ displays a similar overshoot, increasing to some $\approx 10\%$ to $\approx 20\%$ above resting values before gradually returning to normal.

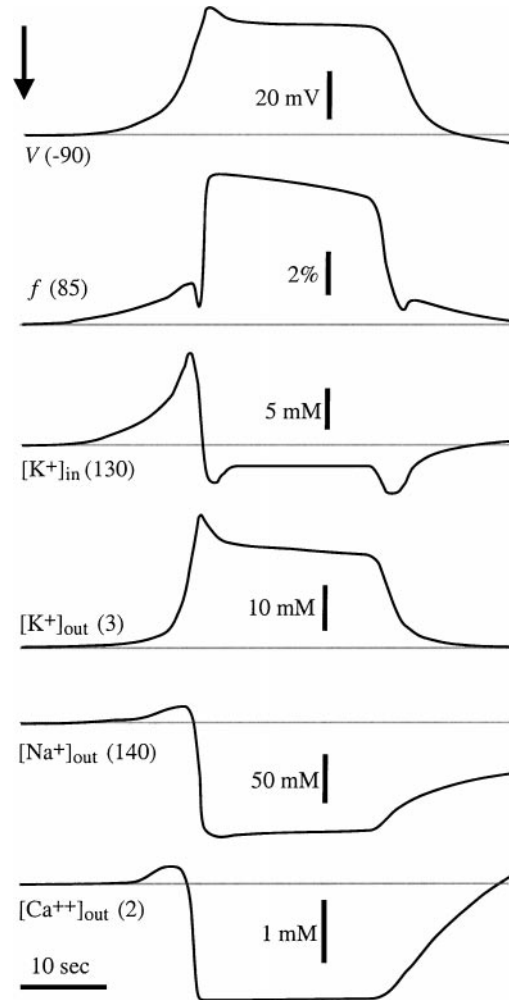


Figure 2. Comparison of DC-voltage shift, volume changes, and ionic concentration shifts observed as a function of time at a fixed point 1 mm from the stimulation. The arrow indicates the stimulation time. The straight lines indicate values at rest (shown in parentheses). Parameters used: $d = 2$, $g_A = 5$, $g_{BK} = 300$, $g_{DR} = 400$, $g_F = 10$, $g_{HVA} = 2$, $g_{IK} = 0$, $g_{LVA} = 0.2$, $g_M = 10$, $g_{NMDA} = 300$, $g_P = 0.1$, $g_{SK} = 0$.

Prior to the rapid loss of $[Na^+]_{out}$, $[Cl^-]_{out}$ and $[Ca^{++}]_{out}$ there is gradual increase in the concentrations of these species to $\approx 10\%$ above their resting levels. This increase is caused (in the simulations) by cellular expansion. As illustrated in Fig. 2, a cytoplasmic pulse of increased $[K^+]_{in}$ (to $\approx 8\%$ above resting levels, ≈ 141 mM in the particular simulation shown in Fig. 2) precedes the major interstitial concentration changes. The peak of the $[K^+]_{in}$ pulse precedes the

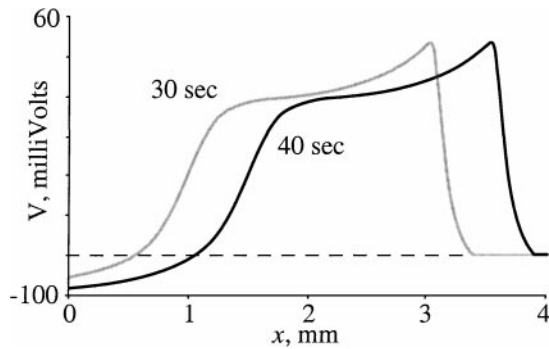


Figure 3. Example of traveling DC-voltage waveform plotted as a function of position at two different times. The initial stimulation is applied at $x = 0$, and the wave is traveling to the right at ≈ 5.9 mm/min. The dashed line indicates the resting potential. Parameters used: $d = 3$, $g_A = 25$, $g_{BK} = 250$, $g_{DR} = 250$, $g_F = 40$, $g_{HVA} = 5$, $g_{IK} = 2$, $g_{LVA} = 0.5$, $g_M = 10$, $g_{NMDA} = 250$, $g_P = 0.4$, $g_{SK} = 0$.

peak of the $[K^+]_{out}$ wave by ≈ 2 sec. This induces early osmotic pressure gradients that are countered by water movement into the cell. Subsequently, $[K^+]_{in}$ falls to $\approx 5\%$ below resting levels (to ≈ 125 mM in the simulation shown in Fig. 2). Cell volume, which had gradually increased by $\approx 2\%$ (reducing interstitial space by $\approx 13\%$) during this $[K^+]_{in}$ pulse, falls by $\approx 1\%$. This transient volume decrease is reversed before the cell can return to its resting volume because depolarization-driven charge movement has begun. As the major wave front passes, cell volume rapidly increases by $\approx 7\%$ (reducing interstitial space by $\approx 50\%$).

The spatial characteristics a typical traveling wave predicted by the model are illustrated in Fig. 3. The DC-voltage shift is plotted as a function of position at two different times following stimulation. The waveform shown is traveling to the right at ≈ 5.9 mm/min. The actual wave speed and magnitude depend on the particular combination of membrane conductances used in a particular simulation. In this simulation a rapid depolarization by ≈ 50 mV occurs at the leading edge of the wave. The leading edge is first followed by a decline of ≈ 10 mV that is spread over a distance of ≈ 0.5 mm. A plateau of ≈ 1.5 mm width trails this initial decline. Repolarization occurs at the trailing edge, which is spread over the next three-quarters of a mm. The start of the trailing hyperpolarization can be seen in the trailing (left) edge of both waveforms in Fig. 3. The DC-voltage waveform illustrated in Fig. 3 has a similar shape to those that have been reported experimentally.

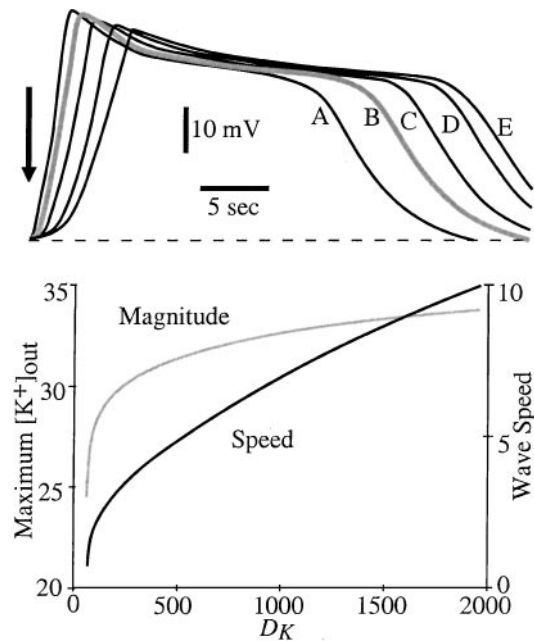


Figure 4. Effect of gap junction block on SD wave propagation. Top: DC-voltage waveform for progressive levels of block. (A) $D_{K,in} = 1960$ (value in free space, shown for reference). (B) Control (heavy gray curve, $D_{K,in} = 980$). (C) 50% block ($D_{K,in} = 490$). (D) 80% block ($D_{K,in} = 196$) (E) 90% block ($D_{K,in} = 98$). Bottom: Wave magnitude and wave speed as a function of cytosolic diffusion constant. A value of $D_{K,in} = 0$ corresponds to 100% gap junction block. Parameter values: $D_{Ca,in} = 200$, $D_{Cl,in} = 508$, $D_{Na,in} = 332$, $g_A = 0$, $g_{BK} = 250$, $g_{DR} = 250$, $g_F = 40$, $g_{HVA} = 4$, $g_{IK} = 1$, $g_{LVA} = 0.4$, $g_M = 0$, $g_{NMDA} = 250$, $g_P = 0.4$, $g_{SK} = 1$.

3.3. Simulated Gap-Junction Block Prevents SD

The predicted effect of gap-junction blocking agents is illustrated in Fig. 4. Block was simulated by progressively reducing the effective cytosolic diffusion constant in successive simulations. Complete block is obtained in this method of analysis by setting all cytoplasmic diffusion constant equal to zero. The model predicts a graded effect, with wave magnitude, wave speed, and wave onset slope all decreasing, and duration of the voltage shift increasing with increasing levels of block. For the particular parameter set used for Fig. 4, all of these measures rapidly decreased to zero when the D_K was reduced below $\approx 4\%$ of its value in free solution ($D_{K,F}$). This is illustrated by steep tails on the left edge of the curves on the bottom of Fig. 4. Similar predictions were made by a second set of simulations in which all diffusion constants were varied simultaneously (not shown). Reducing the diffusion

constants of the other species besides K^+ to zero had significantly less influence, with the effect of Na^+ being the most pronounced ($\approx 10\%$ reduction in wave speed and magnitude with $D_{Na} = 0$ compared with $D_{Na} = 332$).

Gap-junction mediated diffusion is strongly dependent on the geometrical distribution of gap junction and may be described by a reduced effective cytoplasmic diffusion constant

$$\frac{D_{in}}{D_{eff}} \approx 1 + 0.0016 \frac{1 - \Delta}{\Delta} \quad (8)$$

in the one-dimensional limit, where Δ is a geometrical measure of the gap-junction distribution, with $\Delta \rightarrow 0$ for highly clumped aggregates of gap junctions and $\Delta \rightarrow 1$ for highly uniform distributions (Keener and Sneyd, 1998, pp. 236–246). In the simulation described in the preceding paragraph, gap-junction mediated SD required $D_K \geq 0.04 D_{K,F}$. If we estimate that the actual cytosolic diffusion constant $D_{K,in}$ is at most 25% of the value in free solution—that is, $D_{K,in} \leq 0.25 D_{K,F}$ —then $D_{in}/D_{eff} \leq 6.25$. With these values Eq. (6) gives $\Delta \geq 0.0003$, indicating that this prediction is compatible with highly clumped aggregates of gap junctions. In other words, for this model to work gap junctions need only to exist in highly localized regions of individual neurons. This interpretation seems likely given the morphology of neurons.

3.4. Interstitial Diffusion is Not Necessary for Wave Propagation

It has been argued that the interstitial diffusion constant should be reduced by a factor of $1/\lambda^2$ from its value in free solution, where λ represents the tortuosity of extracellular space. Values for λ in the CNS typically range from 1.4 to 2.5 (Nicholson and Syková, 1998; Rusakov and Kullman, 1998). Extracellular tortuosity was not included in the model because extracellular diffusion does not play a significant role in the results. Reducing the interstitial diffusion constants of all species to zero reduced the predicted wave magnitude and wave speed by less than 1% in this model (data not shown).

3.5. Effect of Selective Block or Overexpression

To determine which, if any, ionic membrane conductances the model predicts will contribute to spreading depression, each conductance was varied throughout

its physiological range while holding all other conductances fixed. Decreasing the conductance corresponds to simulation of channel block and increasing the conductance corresponds to simulation of channel overexpression. Typical values of these conductances in gray matter are summarized in Table 1. Variation of each parameter produced a continuously graded effect on waveform shape, wave magnitude, and wave speed. The effect of selective block or overexpression on waveform shape for various parameters is illustrated in Fig. 5. Wave magnitude (maximum $[K^+]_{out}$) and propagation velocity (measured as wave-front speed at half-maximal $[K^+]_{out}$) is illustrated in Fig. 6 as a function of parameter value. It was found that waveform shape, wave magnitude, and wave speed depend on the actual combination of membrane conductances present in the tissue. When these parameters were varied over their known physiological ranges, wave speeds ranging from ≈ 2 mm/min to ≈ 18 mm/min were predicted. Wave magnitude varied from ≈ 25 mM to ≈ 60 mM in different simulations. For any given simulation, waves either propagated at a fixed speed and magnitude without changing shape or did not propagate at all.

Not all ionic conductances were predicted to contribute in the same manner to the propagating wave. The delayed rectifier, the BK-channel, and the HVA Ca^+ channel appear to facilitate spreading depression and both the NMDA-channel and the fast Na^+ channel have primarily facilitating properties. At sufficiently low BK, DR or NMDA conductances (but not for low or even zero HVA or Na^+) waves could not be induced at all. However, this “threshold” phenomenon depends on the values other conductances. For example, a given value of g_{DR} may be below threshold for one combination of g_{BK} and g_{NMDA} but not for another combination. The wave speed increases with membrane conductance for all facilitating conductances. Both the NMDA and the Na^+ conductance may limit wave propagation, as wave magnitude decreases somewhat at higher conductances. Wave magnitude increases with conductance for the other facilitating channels.

The effect of selective block on these facilitating conductances is illustrated Fig. 5A–E. Each illustration shows a pair of curves. One represents a control simulation, while the other represents a block simulation. Block is simulated by reducing a single membrane conductance to 10% of its control value. This is equivalent to selectively blocking $\approx 90\%$ of the given channels. The curves give the DC-voltage waveform observed at a fixed point, either 1 mm (DR, BK) or

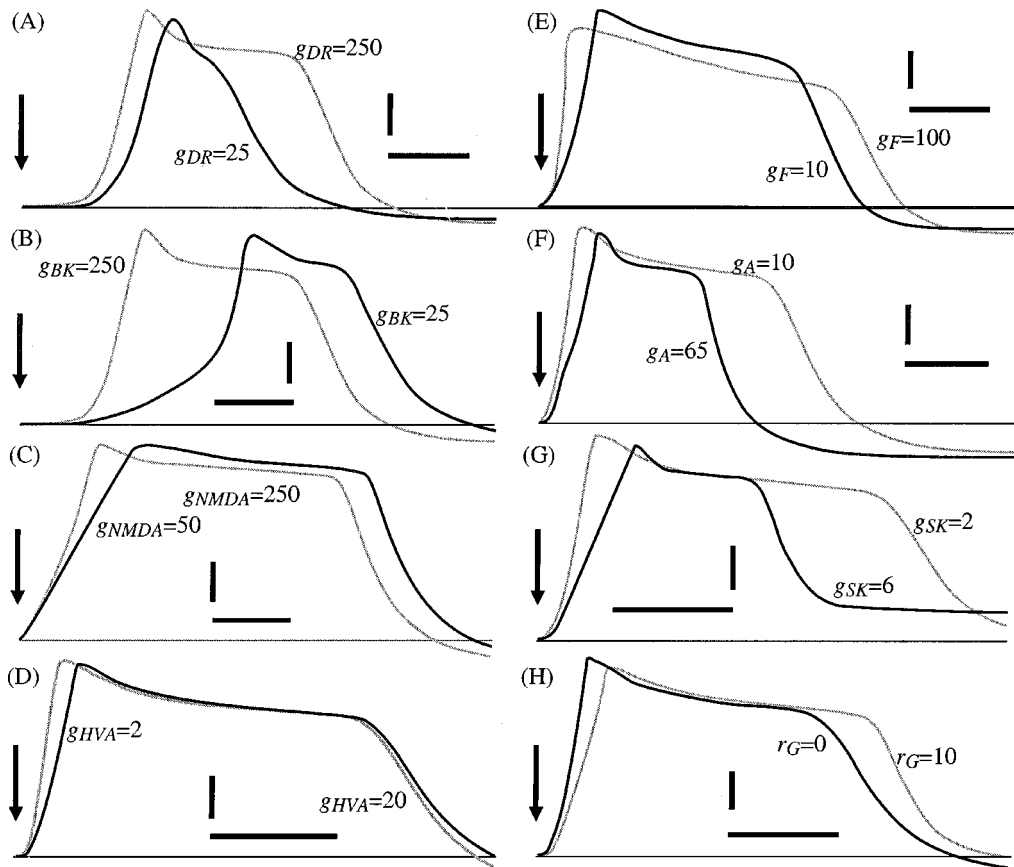


Figure 5. Effect of selective block or overexpression. Each pair of curves shows the DC-voltage shift as a function of time at a fixed point for two different values of a selected parameter with all other parameters held fixed. Arrows indicate stimulation time. The membrane voltage at rest is indicated by horizontal lines. Scale bars: time, 10 sec; voltage, 10 mV. Conductances used: (A) $g_{BK} = 250$, $g_{NMDA} = 250$, $g_{HVA} = 4$, $g_{LVA} = 0.4$, $g_F = 10$, $g_P = 0.1$; (B) $g_{DR} = 250$, $g_{NMDA} = 250$, $g_{HVA} = 4$, $g_{LVA} = 0.4$, $g_F = 10$, $g_P = 0.1$; (C) $g_{DR} = 300$, $g_{HVA} = 2$, $g_{LVA} = 0.2$, $g_F = 10$, $g_P = 0.1$; (D) $g_{DR} = 250$, $g_A = 25$, $g_M = 10$, $g_{BK} = 250$, $g_{IK} = 2$, $g_{SK} = 2$, $g_{NMDA} = 250$, $g_F = 40$, $g_P = 0.1$; (E) $g_{DR} = 1000$, $g_A = 10$, $g_M = 10$, $g_{NMDA} = 100$, $g_{HVA} = 4$, $g_{LVA} = 0.4$, $g_F = 40$, $g_P = 0.4$; (F) $g_{DR} = 25$, $g_{BK} = 250$, $g_{NMDA} = 250$, $g_{HVA} = 4$, $g_{LVA} = 0.4$, $g_F = 40$, $g_P = 0.4$; (G) $g_{DR} = 250$, $g_{BK} = 250$, $g_{NMDA} = 250$, $g_{HVA} = 4$, $g_{LVA} = 0.4$, $g_F = 10$, $g_P = 0.1$; (H) $g_{DR} = 250$, $g_{BK} = 250$, $g_{NMDA} = 250$, $g_{HVA} = 4$, $g_{LVA} = 0.4$, $g_F = 40$, $g_P = 0.4$.

0.5 mm (NMDA, HVA, Na^+) from the simulation. In each of these cases, blocking the current decreases the onset slope.

Selectively blocking the delayed rectifier (DR, Fig. 5A) also caused the depolarization to end substantially earlier and reduces the magnitude of the repolarization slope. At sufficiently low g_{DR} , the onset-slope and repolarization-slope meet in a somewhat triangularly shaped waveform. At lower values (higher block) waves do not propagate. Both the predicted wave speed and predicted wave magnitude increased smoothly with g_{DR} (Fig. 6A), suggesting that this channel facilitates the propagation of spreading depression.

Selective BK-channel block affects the waveform differently than does selective DR block. The atten-

uation in onset slope is more severe under BK block, resulting in a delay in wave onset. Repolarization is also delayed, although there is no change in the repolarization slope (Fig. 5B). Since repolarization is delayed less than wave onset, the duration of the depolarization decreases with channel block. For some combinations of membrane conductances, at high levels of block this delay in wave onset could surpass the delay in recovery, thereby preventing wave propagation. As block is reduced and g_{BK} is allowed to increase, the wave speed and wave magnitude both increase smoothly (Fig. 6B).

NMDA block reduces both K^+ efflux and Ca^{++} , which in turn reduces activation of $\text{K}(\text{Ca})$ channel and decreases calcium-induced calcium release. Selective block of the NMDA channel decreased the wave-onset

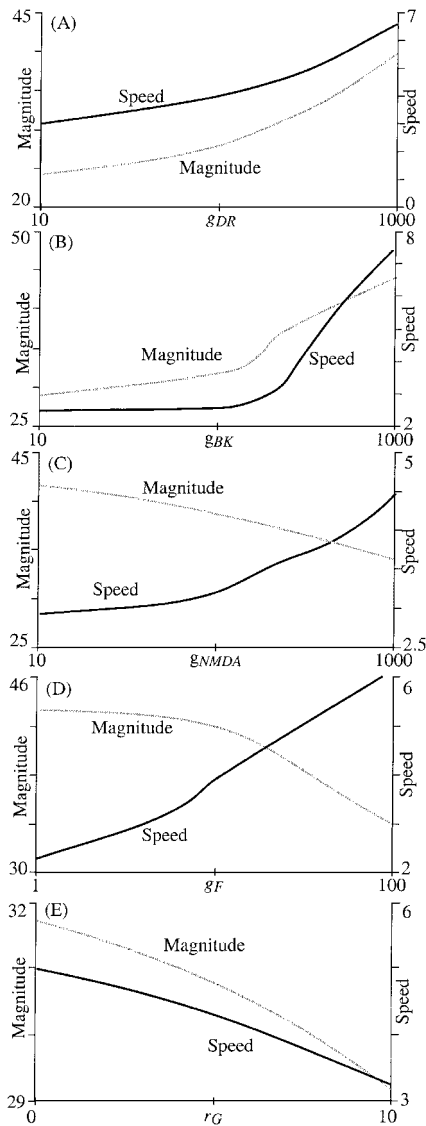


Figure 6. Effect of parametric variation of membrane conductances on wave magnitude and speed. Magnitude is measured as the maximum value of $[K^+]_{out}$ in mM, and speed is in mm/min. The abscissas give conductance in $pS/\mu m^2$ (logarithmic scale, A to D) and glial K^+ pump rate in mm/liter-sec (linear scale). (A) Variation of delayed rectifier membrane conductance. Parameters: $g_{BK} = 250$, $g_{K,NMDA} = 250$, $g_{HVA} = 4$, $g_{LVA} = 0.4$, $g_F = 40$, $g_P = 0.4$. (B) Variation of BK channel membrane conductance. Parameters: $g_A = 50$, $g_{DR} = 300$, $g_M = 10$, $g_F = 10$, $g_P = 0.1$, $g_{HVA} = 4$, $g_{LVA} = 0.4$, $g_{IK} = 4$, $g_{K,NMDA} = 100$. (C) Variation of NMDA membrane conductance. The abscissa gives the K^+ conductance. Parameters: $g_{DR} = 300$, $g_F = 10$, $g_P = 0.1$. (D) Variation of fast Na^+ channel membrane conductance, with $g_P/g_F = 0.01$ (fixed). Other parameters: $g_A = 10$, $g_{DR} = 1000$, $g_M = 10$, $g_{K,NMDA} = 100$. (E) Variation of total glial K^+ pumping rate. Other parameters: $g_{BK} = 250$, $g_{IK} = 1$, $g_{SK} = 1$, $g_{DR} = 250$, $g_F = 40$, $g_P = 0.4$, $g_{K,NMDA} = 250$, $g_{HVA} = 4$, $g_{LVA} = 0.4$.

slope but less severely than BK channel block. Wave recovery was also delayed, but no change in the repolarization slope occurred (Fig. 5C). At high levels of block, SD could not be induced, although the level of block required to prevent SD depends on the values of g_{BK} and g_{DR} , with higher levels of block required at higher values of these other two conductances. As block is reduced (g_{NMDA} increased), wave speed was predicted to increase, as it was for both BK and DR block removal (Fig. 6C). However, and in contrast to both BK and DR channels, predicted wave magnitude decreased as the level of channel block decreased (that is, wave magnitude decreased with increasing g_{NMDA}). Maximum wave magnitude occurred just at threshold (minimum g_{NMDA} or maximum level of block under which SD would propagate). Thus NMDA currents have a mixed facilitating and inhibitory role on SD. They are facilitating in the sense that the larger the NMDA currents, the larger the speed of the wave. NMDA currents are inhibitory, however, in the sense that at higher currents the magnitude of the wave is smaller; this helps to limit the ionic redistributions that occur during SD. However, NMDA currents are primarily facilitating, in that it was usually possible to completely prevent SD by completely blocking NMDA channels (except at high g_{DR} and g_{BK}), while it was not possible to completely block SD by increasing the NMDA conductance.

Selective block of the HVA Ca^{++} current decreased the onset slope and delayed recovery (Fig. 5D). The effect of reducing Ca^{++} currents is to reduce Ca^{++} entry into the cell. In the model, this prevents Ca^{++} -induced Ca^{++} -release from internal stores and reduces the activation levels of $K(Ca)$ channels. For the simulation of Fig. 5D, both the DR and NMDA channels were present at sufficiently high conductances (unblocked) so BK-channel block had very little effect on wave propagation. However, in tissue with very low levels of total NMDA and DR conductance, the resulting effective $K(Ca)$ block could prevent SD propagation. Simulating Ca^{++} removal from the bath by reducing $[Ca^{++}]_{out}$ was predicted to have a similar effect (Fig. 7). This is consistent with observations of a reduction in the wave-onset slope when Ca^{++} was removed from the bath (Basarsky et al., 1998).

Selective block of Na^+ currents reduced onset slope and decreased the length of depolarization while wave magnitude increased (Fig. 5E). In all simulations, the ratio $g_P/g_F = 100$ was held fixed; thus both currents were blocked simultaneously. As block is reduced (g_F and g_P increase) wave magnitude decreases and wave

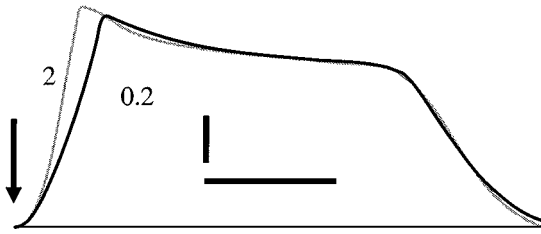


Figure 7. Effect of Ca^{++} reduction in the bath on waveform shape. The DC-voltage waveform is shown as a function of time at a fixed point 0.5 mm from the stimulation point for two levels of $[\text{Ca}^{++}]_{\text{out}}$ (indicated in mM on the figure). The arrow indicates the stimulation time and the horizontal line the resting membrane potential. Scale bars: 10 sec, 10 mV. Parameter values: same as Fig. 5D.

speed increases (Fig. 6D). Thus while Na^+ currents are predicted to facilitate SD in the sense that they make the wave propagate faster, they have a limiting effect by controlling wave magnitude. It has been observed that in some preparations SD can be induced by blocking inactivation of the sodium channel (Ashton et al., 1997), while a complete block of both calcium and sodium channels has been observed to prevent SD-like hypoxic depolarizations (Müller and Somjen, 1998). Thus Na^{++} currents appear to have a primarily facilitating influence on SD.

The SK channel and A-type K^+ current were predicted to have purely inhibitory influences on SD, with both wave magnitude and wave speed decreasing with increasing membrane conductance. Instead of a threshold (minimum) value, these conductances exhibited a cutoff (maximum) value, above which SD could not be induced. Completely blocking either of these conductances increased both wave magnitude and wave speed. Increasing either of these conductances, as might occur if the proteins were overexpressed, severely attenuated wave propagation. The effect of overexpression on the shape of the DC-voltage waveform as observed at a fixed point 0.5 mm from the stimulation is illustrated for the A-type K^+ channel in Fig. 5F and for the SK-channel in Fig. 5G. In both cases, as the conductance increased, both the onset slope and the duration of the depolarization decreased. For the particular parametric combinations illustrated in Fig. 5, the two edges of the waveform “came together” above $g_A \approx 70$ and $g_{SK} \approx 7$, above which values SD could not be induced. The interpretation of the A-channel as an inhibitory influence on SD is consonant with reports of spontaneous spreading following the application 4-AP (Psarropoulou and Avoli, 1993; Avoli et al., 1996). In other experiments, seizure had been observed follow-

ing the application of apamin (McCown and Breese, 1990). The prediction of increased susceptibility to SD under SK-channel block is consistent with this observation of 4-AP-induced seizure if both SD and seizure occur as a result of related mechanisms. SD has also been reported following the application of other convulsive agents at subconvulsive dosages (Hablitz and Heinemann, 1989; Koroleva et al., 1993).

Simulated block of the other ion channels included in the model (M, IK, and LVA currents) produced no observable effect on waveform shape, wave speed, or wave magnitude. Each conductance was varied over its physiological range to determine if any effect could be discerned. Parametric ranges are indicated in the appendix.

Selective glial block was simulated by reducing the total glial pump rate to zero. The DC-voltage waveform is shown in Fig. 5H. At complete block, the onset slope increased while the duration of depolarization decreased. Maximum wave speed and wave magnitude occurred when glial cells were completely blocked (Fig. 6E). Removing block causes a smooth decrease in wave speed and wave magnitude. These predictions are consistent with the interpretation of glial cells as protecting neural tissue against spreading depression as they try to maintain interstitial homeostasis. The prediction that glial block will not prevent spreading depression is also consonant with observations (Largo et al., 1996, 1997b).

3.6. Osmotic Expansion Is Required for SD

To determine if cellular expansion is necessary for SD in this model, the maximum allowed reduction in extracellular space (ECS) was varied by parametrically changing the value of f_{max} in Eq. (5). The allowed reduction in ECS (ΔECS_{max}) was varied from 0% (no reduction, completely rigid cells) to 90%. Waves could not be induced unless the cells were allowed to expand. This is illustrated in Fig. 8 for two different values of the resting neuronal volume fraction f . There is a sharp threshold in ΔECS_{max} at $\approx 15\%$ to $\approx 20\%$ for the parameter set used in this set of simulations. For $\Delta ECS_{\text{max}} < \approx 15\%$ to $\approx 20\%$ SD did not occur, while for $\Delta ECS_{\text{max}} > \approx 15\%$ to $\approx 20\%$ SD could be induced. As ΔECS_{max} was raised above $\approx 15\%$ to $\approx 20\%$ a steep increase in wave speed to a plateau of ≈ 3 mm/min occurred. The actual level of the plateau varied with membrane conductance. As ΔECS_{max} was raised beyond $\approx 40\%$ no further change in wave speed was

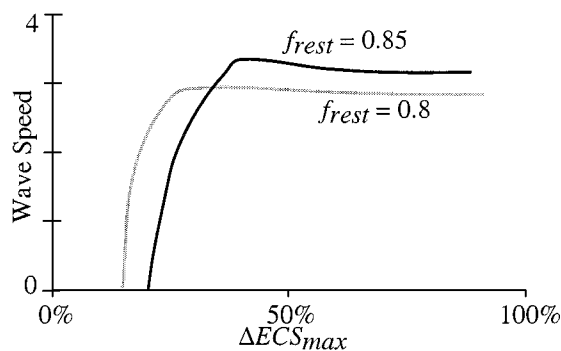


Figure 8. Effect of limiting the allowed reduction in extracellular space ΔECS_{max} . The wave speed is shown as a function of ΔECS_{max} for two different values of the resting neuronal volume fraction.

predicted. Thus cells need to expand to occupy some 15% to 40% of the interstitial volume to allow wave passage. If spreading depression has a neuroprotective function, this might give an evolutionary advantage for organisms without a tightly packed neuropil.

4. Discussion

The goals of this study were (1) to model a putative mechanism (electrodiffusion) for gap-junction mediated propagation of spreading depression and (2) to evaluate the contribution of osmotic forces to SD wave propagation. The first goal was inspired by several experiments in which spreading depression was inhibited by selectively blocking gap junctions, while glial poisons do not prevent SD (Martins-Ferreira and Ribeiro, 1995; Nedergaard et al., 1995; Largo et al., 1997b; Aitken et al., 1998b). The aim was to model a way in which SD might propagate via neuronal gap junctions; gating mechanisms were deemed beyond the scope of this study. The second goal was based on the observations of substantial neuronal volume changes during SD (Kraig and Nicholson, 1978; Jing et al., 1994). It is not known if these volume changes are necessary for wave propagation. Osmotic forces and the consequent volumetric changes have not been included in any previous mathematical model of spreading depression.

The simulations suggested that spreading depression will not propagate unless there is sufficient space for cellular expansion. It has been reported anecdotally that SD is more difficult to induce in species with a more convoluted cortex (for example, in humans). It is intriguing to speculate that the reason for this may

be, in fact, that the neuropil is more tightly packed in these species. This may provide species with less tightly packed cortex, such as reptiles and fish, some protection against seizure.

Three assumptions were crucial in this model. The first assumption is based on the observations that interstitial space contracts during SD, thereby increasing $[K^+]_{out}$ (Jing et al., 1994). The most likely mechanism for such expansion is osmosis. Changing the ionic content of a cell leads to the generation of osmotic pressure gradients. To relieve these gradients water passes across the cell membrane causing it to either expand or contract. If the cells are not allowed to expand in the present model, the depolarization-induced potassium efflux is insufficient to induce a propagating wave.

The second crucial assumption is that cytosolic ionic movements must be described electrodiffusively and not by a traditional ohmic (such as a compartmental, cable equation-based) approach. The assumption that significant concentration changes do not occur is implicit in the derivation of the cable equation; this assumption is clearly not valid during spreading depression. When all concentration changes are small, as is presumably the case during normal physiological behavior, the membrane voltage calculated electrodiffusively is almost indistinguishable from that predicted with a traditional compartmental approach (Qian and Sejnowski, 1989). Thus there is normally no reason to consider electrodiffusion. However, the model predicts that electrodiffusive forces will generate a cytosolic K^+ pulse preceding the other ionic changes that occur during SD, while depolarization causes substantial Na^+ and Cl^- fluxes into cells. The resulting osmotic forces lead to water entry and sufficient cellular expansion to induce a regenerative wave of spreading depression.

The third crucial assumption is that a sufficient level of open interneuronal gap junctions are present in neuronal tissue. How gap junctions activate during wave passage is beyond the scope of the present study and remains a factor that should be examined more closely. This does not detract from the present results, since they suggest that an SD-like wave can be propagated via cytosolic transport if there is some mechanism that will open the gap junctions and if the cell is allowed to expand and contract in response to osmotic forces. It has been speculated that a wave of spreading depression causes normally closed gap junctions between neurons to open by some yet to be determined mechanism (Somjen et al., 1992). This view was taken here. There is some evidence indicating the widespread

presence of gap-junctional proteins in the CNS, particularly during early development (Sloper and Powel, 1978; Bayer and Pickel, 1990; Bozhilova-Pastirova and Ovtcharoff, 1995; Simbürger et al., 1997). These may be necessary for the organization of neural circuits (Peinado et al., 1993; Kandler and Katz, 1995; Rörig et al., 1995). It is not known if these gap junctions are normally open or closed.

The high-speed (AC) voltage spikes that precede an approaching SD wave have been completely ignored in this model. Various observations have suggested that these spikes can be blocked by the application of sodium channel blockers without otherwise significantly affecting the DC-voltage shift that occurs during SD (Herreras et al., 1994). This suggests that whatever mechanism causes the spikes can be dissociated from the mechanisms that induces the DC-voltage change. The hypothesis that has been made in the present article is that spikes result from axonal Na^+ currents. The typical Na^+ channel density used in this model was ≈ 5 channels/ μm^2 , corresponding to measurements in gray matter. Since axonal Na^+ channel densities are substantially higher, approaching 2000 channels/ μm^2 at nodes of Ranvier (Hille, 1992), it seems likely that such spikes would occur if an axonal compartment were added to the model. The role of spikes during spreading depression remains an important issue for further study.

The simulations also show that standard electrophysiological models may be used to describe the DC-voltage shift and ionic redistribution that occurs during spreading depression—or at least during a variety of spreading depression-like phenomena. Propagation velocity and waveform shape depend on the specific combination of ion channels present in the tissue. In particular, facilitating roles were predicted for the delayed-rectifier, BK and NMDA-gated channels, and to a lesser extent, Na^+ and HVA-type Ca^{++} channels, while inhibitory roles were predicted for neuroglia and the A and SK channels. These proteins are all present at varying levels in different types of neural tissue. Consequently, the partial or complete block of SD by NMDA-R antagonists (Hernandez-Caceres et al., 1987; Lauritzen et al., 1988; Marrannes et al., 1988; Lauritzen and Hansen, 1992; McLachlan, 1992; Nellgard and Wieloch, 1992), Magnesium (Mg^{++}) ions (van Harrevel, 1984; Lauritzen et al., 1988) and tetraethylammonium (TEA) ions (Scheller et al., 1998) can be explained. Furthermore, the presence of voltage-gated Ca^{++} channel antagonists or the removal of interstitial

Ca^{++} will inhibit spreading depression only if the appropriate combination of ion channels is present. In all cases, poisoning gap junctions (such as by reducing the cytosolic diffusion coefficient to zero) will inhibit spreading depression.

Appendix

Implementation

Equations (1) and (2) are written in the general form

$$\frac{\partial c}{\partial t} = \frac{\partial}{\partial x} \left(D \frac{\partial c}{\partial x} \right) + g(x, t), \quad (9)$$

where

$$g(x, t) = \begin{cases} \frac{zF}{RT} \frac{\partial}{\partial x} \left(c_{in} D_{c,in} \frac{\partial E}{\partial x} \right) - \kappa J_{c,m} + s_c, & \text{cytoplasmic} \\ \frac{\kappa f}{1-f} J_{c,m} - J_{c,glia}, & \text{interstitial} \end{cases} \quad (10)$$

The membrane ion flux $J_{c,m}$ for each species is just the simple sum of the ion fluxes for all currents for that species. Equation (10) was solved numerically using the Crank-Nicholson method (Morton and Mayers, 1994). The implicit difference formula for the concentration at time-step $n + 1$ and grid point j is

$$\begin{aligned} & \frac{C_j^{n+1} - C_j^n}{\Delta t} \\ &= \frac{1}{2(\Delta x)^2} \left[D_{j+1/2}^{n+1} (c_{j+1}^{n+1} - c_j^{n+1}) \right. \\ & \quad \left. - D_{j-1/2}^{n+1} (c_j^{n+1} - c_{j-1}^{n+1}) + D_{j+1/2}^n \right. \\ & \quad \left. \times (c_{j+1}^n - c_j^n) - D_{j-1/2}^n (c_j^n - c_{j-1}^n) \right] \\ & \quad + \frac{1}{2} [g_j^{n+1} + g_j^n], \end{aligned} \quad (11)$$

where $D_{j+1/2}^n$ is the diffusion constant evaluated at a spatial location halfway between grid points j and $j + 1$. To account for voltage-dependent gap-junctional conductivity or calcium block, $D_{j+1/2}^n$ is calculated using a standard cubic-spline interpolation scheme. Since Eq. (11) is implicit in g_j^{n+1} , c_j^n was used to obtain a first estimate of g_j^{n+1} on the right side of the equation. Iteration for successive approximations to g_j^{n+1} was

continued at each time step until the membrane voltage converged to within 10^{-7} mV.

Ion Currents

All ion currents are described by standard biophysical models. The Hodgkin-Huxley formalism (1952) is used to describe ionic currents as

$$j = gm^p h^q (V - V_c), \quad (12)$$

where g is the membrane conductance, m and h describe channel activation and inactivation, respectively, $V_c = (RT/zF) \ln(c_{out}/c_{in})$ is the Nernst potential for species c , and p and q are integers that are prespecified and fixed for each type of channel. For Ca^{++} , Eq. (12) is replaced by a Hodgkin-Huxley-Goldman hybrid (see below). The activation and inactivation variables relax exponentially to their steady-state values x_∞ (where $x = h$ or $x = m$) according to

$$\frac{dx}{dt} = \frac{x_\infty - x}{\tau_x}. \quad (13)$$

Both τ_x and x_∞ may be concentration and/or voltage dependent. In some cases, explicit formulas are given; in other cases, τ_x and x_∞ are given in terms of forward and backward rate constants α_x and β_x between putative closed and open states, where

$$\tau_x = \frac{1}{\alpha_x + \beta_x} \quad (14)$$

$$x_\infty = \frac{\alpha_x}{\alpha_x + \beta_x}. \quad (15)$$

A passive Cl^- flux is calculated to balance the cation flux since it is the only membrane-permeant anion included in the model.

The specific equations and parameters used are given in the following paragraphs. To simplify the equations, channel currents are given rather than channel fluxes. To convert to a flux, each current should be divided by F (Faraday's constant, ≈ 96 Coulombs/mM). The following notation is used: C , Ca^{++} concentration; Cl , Cl^- concentration; I , IP3 concentration; K , K^{++} concentration; N , Na^+ concentration; $R = 8.314$ Joules/mole-Kelvin; $T =$ temperature, Kelvin; V , membrane potential; V_c , Nernst potential for species c ; $z =$ valence; $\varphi = zFV/RT$. The subscripts in, out and ER refer to concentrations in the cytosol, interstitial region, and endoplasmic reticulum, respectively.

Parameter values used are derived from observed conductances in gray matter (see Table 1).

Gap Junctions

$$D_{c,in} = D_0 \gamma(V) B([\text{H}^+], [\text{Ca}^{++}])$$

$$\gamma(\Delta V) = \frac{2}{\exp\left(\frac{-\Delta V/V_H}{1+e^{\Delta V/V_H}}\right) + \exp\left(\frac{\Delta V/V_H}{1+e^{-\Delta V/V_H}}\right)}$$

$$V_H = \approx 40 \text{ to } \approx 1000 \text{ mV}$$

$$B([\text{H}^+]_{in}, [\text{Ca}^{++}]_{in}) = \frac{R_{Ca}^n (1 + R_H)^{2n}}{1 + R_{Ca}^n (1 + R_H)^{2n}}, n = 3$$

$$R_{Ca} = K_{Ca}/[\text{Ca}^{++}]_{in}, K_{Ca} = 316 \text{ nM}$$

$$R_H = K_H/[\text{H}^+]_{in}, K_H = 112 \text{ nM}$$

A-Channel K^+ Current

$$j_A = g_A m h (V - V_K)$$

$$m_\infty = \frac{1}{1 + e^{-(V+42)/13}}$$

$$h_\infty = \frac{1}{1 + e^{(V+110)/18}}$$

$$\tau_m = 0.00138$$

$$\tau_h = \begin{cases} 0.050, & V < -80 \\ 0.150, & V \geq -80 \end{cases}$$

$$g_A = 0 \text{ to } 100$$

M-Channel K^+ Current

$$j_M = g_M m (V - V_K)$$

$$m_\infty = \frac{1}{1 + e^{-(V+35)/10}}$$

$$\tau_m = \frac{1}{3.3[e^{(V+35)/40} + e^{-(V+35)/40}]}$$

$$g_M = 0 \text{ to } 100$$

Delayed Rectifier K^+ Current

$$j_{DR} = g_{DR} m^2 h (V - V_K)$$

$$m_\infty = \frac{\alpha(V - 20)}{\alpha(V - 20) + \beta(V - 20)}$$

$$\alpha(V) = \frac{0.0047(V + 12)}{1 - e^{-(V+12)/12}}$$

$$\beta(V) = e^{-(V+147)/30}$$

$$h_{\infty} = \frac{1}{1 + e^{(V+25)/4}}$$

$$\tau_h = \begin{cases} 0.006, & V < -25 \\ 0.050, & V > -25 \end{cases}$$

$$g_{DR} = 0 \text{ to } 2000$$

BK-Channel K(Ca) Current

$$j_{BK} = g_{BK}m(V - V_K)$$

$$m_{\infty} = \frac{250C_{in}e^{V/24}}{250C_{in}e^{V/24} + 0.1e^{-V/24}}$$

$$\tau_m = \frac{0.001}{250C_{in}e^{V/24} + 0.1e^{-V/24}}$$

$$g_{BK} = 0 \text{ to } 1000$$

IK-Channel K(Ca) Current

$$j_{IK} = \frac{gm(V - V_K)}{(1 + 0.0002/C_{in})^2}$$

$$\alpha_m = 25$$

$$\beta_m = 0.075e^{(V+5)/10}$$

SK-Channel K(Ca) Current

$$j_{SK} = g_{SK}m^2(V - V_K)$$

$$m_{\infty} = \frac{1.25 \times 10^8 C_{in}^2}{1.25 \times 10^8 C_{in}^2 + 2.5}$$

$$\tau_m = \frac{1}{1.25 \times 10^8 C_{in}^2 + 2.5}$$

$$g_{SK} = 0 \text{ to } 10$$

LVA Ca⁺⁺ Current

$$j_{LVA} = 2\phi g_{LVA}pmh \frac{C_{in}e^{\phi} - C_{out}}{e^{\phi} - 1}$$

$$\alpha_m = \frac{2.6}{1 + e^{-(V+21)/8}}$$

$$\alpha_h = \frac{0.0025}{1 + e^{(V+40)/8}}$$

$$\beta_m = \frac{0.018}{1 + e^{(V+40)/4}}$$

$$\beta_h = \frac{0.19}{1 + e^{-(V+50)/10}}$$

$$g_{LVA} = 0 \text{ to } 2; p = 1.2 \times 10^{-5} \text{ (cm/sec)/(pS/}\mu\text{m}^2)$$

HVA Ca⁺⁺ Current

$$j_{HVA} = 2\phi g_{HVA}pmh \frac{C_{in}e^{\phi} - C_{out}}{e^{\phi} - 1}$$

$$\alpha_m = \frac{8.5}{1 + e^{-(V-8)/12.5}}$$

$$\alpha_h = \frac{0.0015}{1 + e^{(V+29)/8}}$$

$$\beta_m = \frac{35}{1 + e^{(V+74)/14.5}}$$

$$\beta_h = \frac{0.0055}{1 + e^{-(V+23)/8}}$$

$$g_{HVA} = 0 \text{ to } 20; p = 1.5 \times 10^{-5} \text{ (cm/sec) (pS/}\mu\text{m}^2)$$

Fast Na⁺ Current

$$j_F = g_Fmh(V - V_{Na})$$

$$\alpha_m = 35e^{(V+5)/10}$$

$$\alpha_h = \frac{0.225}{1 + e^{(V+80)/10}}$$

$$\beta_m = 7e^{-(V+65)/20}$$

$$\beta_h = 7.5e^{(V-3)/18}$$

$$g_F = 0 \text{ to } 100$$

Persistent Na⁺ Current

$$j_P = g_Pm(V - V_{Na})$$

$$\alpha_m = \frac{200}{1 + e^{-(V-18)/16}}$$

$$\beta_m = \frac{25}{1 + e^{(V+58)/8}}$$

$$g_P = 0 \text{ to } 1$$

NMDA Currents

$$j_{NMDA} = g_{c,NMDA}A([Glu], V)B([Mg^{++}], V)$$

$$\times V \frac{(c_{in}/c_{out})e^{\phi} - 1}{e^{\phi} - 1}, c = C, K, N$$

$$A([Glu], V) = \frac{\alpha[Glu]}{\alpha[Glu] + \beta}, \alpha = 72 \text{ mM}^{-1} \text{ sec}^{-1},$$

$$\beta = 6.6 \text{ sec}^{-1}$$

$$[\text{Glu}] = \frac{T_{\max}}{1 + e^{-(V-2)/5}}$$

$$B([\text{Mg}^{++}], V) = \frac{1}{1 + 0.028M e^{-0.062V}}$$

$$g_{c,\text{NMDA}} = \frac{PF^2 z^2}{RT} c_{\text{out}}$$

$$P_{\text{Ca}}/P_{\text{K}} = 3.0 \text{ to } 10.6; \quad P_{\text{Na}}/P_{\text{K}} = 1.0;$$

$$T_{\max} = 1; \quad M = 1$$

Leak Currents

$$j_{\text{Leak}} = PzF\phi \frac{c_{\text{in}} - c_{\text{out}} e^{-\phi}}{1 - e^{-\phi}}, \quad c = C, K, N$$

Na, K Pump Currents

$$j_{\text{K}} = -r_{\text{Na,K}} \left(\frac{K_{\text{out}}}{K_{\text{out}} + 3.7} \right)^2 \left(\frac{N_{\text{in}}}{K_{\text{in}} + 0.6} \right)^3$$

$$\times \frac{0.052 \sinh \Phi}{0.026 e^{\Phi} + 22.5 e^{-\Phi}}$$

$$j_{\text{Na}} = \frac{3}{2} j_{\text{K}}$$

$$\Phi = \frac{F}{RT} (V + 176.5)$$

Na, Ca Pump Current

$$j_{\text{Ca}} = \frac{r_{\text{Na,Ca}}}{r_0^4}$$

$$\times \frac{N_{\text{in}}^3 C_{\text{out}} \exp(0.02V) - N_{\text{out}}^3 C_{\text{in}} \exp(-0.02V)}{1 + 0.0001(N_{\text{out}}^3 C_{\text{in}} + N_{\text{in}}^3 C_{\text{out}})}$$

$$j_{\text{Na}} = -\frac{3}{2} j_{\text{Ca}}$$

$$r_{\text{Na,Ca}} = 0.2 \mu\text{A}/\text{cm}^2; \quad r_0 = 12 \text{ mM}$$

Ca ATPase Current

$$j_{\text{Ca}} = r_{\text{ATP}} \frac{C_{\text{in}}}{C_{\text{in}} + 0.0002}; \quad r_{\text{ATP}} = 0.2 \mu\text{A}/\text{cm}^2$$

HCO₃, Cl Exchanger Current

$$j_{\text{Cl}} = r \frac{Cl_{\text{in}}}{Cl_{\text{in}} + 4}, \quad r = 0 \text{ to } 5 \mu\text{A}/\text{cm}^2$$

Na, K, Cl Cotransporter Currents (Glia)

$$j_{\text{K}} = r_{\text{Na,K,Cl}} \left(\frac{K_{\text{out}}}{K_{\text{out}} + 2.7} \right)$$

$$\times \left(\frac{N_{\text{out}}}{N_{\text{out}} + 25} \right) \left(\frac{Cl_{\text{out}}^2}{Cl_{\text{out}}^2 + 1600} \right)$$

$$j_{\text{Na}} = j_{\text{K}}; \quad j_{\text{Cl}} = -2j_{\text{K}}; \quad r_{\text{Na,K,Cl}} = 0 \text{ to } 1 \text{ mM}/\text{sec}$$

ER Ca⁺⁺ Pump

$$j_{\text{Pump}} = v_{\text{ER}} \frac{C_{\text{in}}}{C_{\text{in}} + 0.001}; \quad v_{\text{ER}} = 2.5 \mu \text{ M}/\text{sec}.$$

Ryanodine Channels

$$j_{\text{R}} = v_{\text{R}} m_{\text{R}} [C_{\text{ER}} - C_{\text{in}}]; \quad v_{\text{R}} = 0.1 \text{ sec}^{-1}$$

$$m_{\text{R},\infty} = \left[1 + \frac{0.05}{C_{\text{in}}} + \frac{C_{\text{in}}}{0.001} \right]^{-1}$$

$$\tau_{\text{R}} = \left[0.8 + \frac{800 C_{\text{in}}}{1 + 0.5/C_{\text{in}}} \right]^{-1}$$

IP3-Dependent Ca⁺⁺ Channels (ER)

$$j_{\text{I}} = r_{\text{I}} h \left(0.567 + \frac{0.433I}{0.004 + I} \right)$$

$$\times \left(0.111 + \frac{0.889C_{\text{in}}}{0.0007 + C_{\text{in}}} \right)$$

$$h_{\infty} = [1 + (C_{\text{in}}/0.0007)^2]^{-1}$$

$$r_{\text{P}} = 40 \mu\text{M}/\text{sec}$$

IP3 Production

$$\frac{dI}{dt} = 0.04h\Delta A - \frac{0.0008I}{0.001 + I}$$

$$h_{\infty} = \begin{cases} 1, & I < 0.0018 \\ 0, & I > 0.0018 \end{cases}$$

Stretch Channels

$$Q_{\text{open}} = q_{\text{max}} [1 + e^{-(\Delta P - \Delta P_{1/2})/K}]^{-1}$$

$$\Delta P = P_{\text{rest}} (f/f_{\text{rest}} - 1)$$

$$P_{\text{rest}} = 760 \text{ mm Hg}; \quad f_{\text{rest}} = 0.85$$

$$K = 10.2 \text{ mm Hg (BK)}; \quad 10 \text{ mm Hg (DR)}$$

$\Delta P_{1/2} = 66$ mm Hg (BK); 80 mm Hg (DR)

$q_{max} = 0.43$ (DR); 0.25 (DR)

Resting Concentrations

$C_{in} = 0.0001$; $C_{out} = 2$; $C_{ER} = 2$

$K_{in} = 130$; $K_{out} = 3$

$N_{in} = 10$; $N_{out} = 140$

$Cl_{in} = 4$; $Cl_{out} = 124$

$I = 0.0018$

Diffusion Constants

$D_{K,out} = 1960$; $D_{K,in} = 490$

$D_{N,out} = 1330$; $D_{N,in} = 330$

$D_{C,out} = 790$; $D_{C,in} = 200$

$D_{Cl,out} = 2030$; $D_{Cl,in} = 500$

Acknowledgments

This research was supported by a systems and integrative biology training grant from the National Institute of General Medical Sciences. Dr. G.G. Somjen suggested studying neuronal gap junctions in connection with spreading depression. Dr. J. Sneyd suggested the diffusional approach to modeling gap junctions. Dr. C.M. Newton and Dr. H. Qian provided much needed advice on the intricacies of mathematical modeling during the course of this research. Dr. M.M. Eiland critically read the manuscript and provided many useful suggestions.

References

- Aitken PG, Borgdorff AJ, Jutta AJA, Kiehart DP, Somjen GG, Wadman WJ (1998a) Volume changes induced by osmotic stress in freshly isolated rat hippocampal neurons. *Pflugers Arch.* 436:991–998.
- Aitken PG, Tombaugh GC, Turner DA, Somjen GG (1998b) Similar propagation of SD and hypoxic SD-like depolarization in rat hippocampus recorded optically and electrically. *J. Neurophysiol.* 80:1514–1521.
- Ashton D, Willems R, Wynants J, Van Reempts J, Marrannes R, Clincke G (1997) Altered Na(+)-channel function as an in vitro model of the ischemic penumbra: Action of lubeluzole and other neuroprotective drugs. *Brain Res.* 745:210–221.
- Atri, A (1996) Mathematical modeling and analysis of intracellular calcium dynamics: Oscillations and wave propagation. PhD diss., University of California, Los Angeles.
- Atri A, Admundson J, Clapham D, Sneyd J (1993) A single-pool model for intracellular calcium oscillations and waves in the *xenopus laevis* oocyte. *Biophys. J.* 65:1727–1739.
- Avoli M, Nagao T, Kohling R, Lucke A, Mattia D (1996) Synchronization of rat hippocampal neurons in the absence of excitatory amino acid-mediated transmission. *Brain Res.* 735:188–196.
- Basarsky TA, Duffy SN, Andrew RD, MacVicar BA (1998) Imaging spreading depression and associated intracellular calcium waves in brain slices. *J. Neurosci.* 18:7189–7199.
- Bayer VE, Pickel VM (1990) Ultrastructural localization of tyrosine hydroxylase in the rat ventral tegmental area: Relationship between immunolabeling density and neuronal associations. *J. Neurosci.* 10:2996–3013.
- Belluardo N, Trovato-Salinaro A, Mudò G, Hurd YL, Condorelli DF (1999) Structure, chromosomal localization, and brain expression of human C × 36 gene. *J. Neurosci. Res.* 57:740–752.
- Berridge MJ (1993) Inositol trisphosphate and calcium signaling. *Nature* 361:315–325.
- Blatz AL, Magleby KL (1987) Calcium-activated potassium channels. *Trends Neurosci.* 10:463–467.
- Bozhilova-Pastirova A, Ovtsharoff W (1995) Structure of the synaptic junctions in the rat sensorimotor cortex: Freeze-etching study of neuronal gap junctions. *Neurosci. Lett.* 201:265–267.
- Bures J, Buresova O, Krivanek J (1974) *The Mechanism and Applications of Leao's Spreading Depression of Electroencephalographic Activity*. Academic Press, New York.
- Burton FL, Hunter OF (1990) Sensitivity to flow of intrinsic gating in inwardly rectifying potassium channel from mammalian skeletal muscle. *J. Physiol. (Lond.)* 424:253–261.
- Christie BR, Eliot LS, Ito K, Miyakawa H, Johnston D (1995) Different Ca⁺⁺ channels in soma and dendrites of hippocampal pyramidal neurons mediate spike-induced Ca⁺⁺ influx. *J. Neurophysiol.* 73:2553–2557.
- Colbert CM, Johnston D (1996) Axonal action-potential initiation and the Na⁺ channel densities in the soma and axon initial segment of subicular pyramidal neurons. *J. Neurosci.* 16:6676–6686.
- De Schutter E, Bower J (1994) An active membrane model of the cerebellar Purkinje cell. I. Simulation of current clamps in slice. *J. Neurophysiol.* 71:375–400.
- De Schutter E, Smolen P (1998) Calcium dynamics in large neuronal network. In: Koch C, Segev I, eds. *Methods in Neuronal Modeling: From Ions to Networks*. MIT Press, Cambridge, MA. pp. 211–250.
- Destexhe A, Mainen ZF, Sejnowski, TJ (1998) Kinetic models of synaptic transmission. In: C Koch, I Segev, eds. *Methods in Neuronal Modeling: From Ions to Networks*. MIT Press, Cambridge, MA. pp. 1–26.
- Di Francesco D, Nobel D (1985) A model of cardiac electrical activity incorporating ionic pumps and concentration changes. *Trans. Roy. Soc. Lond.* B307:353–398.
- Di Polo R, Beaugé L (1979) Physiological role of ATP-driven calcium pump in squid axon. *Nature* 278:271–273.
- Douglas R, Martin K (1998) Neocortex. In: Shepherd GM, ed. *The Synaptic Organization of the Brain* (4th ed.). Oxford University Press, New York.
- Fan J, Walsh KB (1999) Mechanical stimulation regulates voltage-gated potassium currents in cardiac microvascular endothelial cells. *Circ. Res.* 84:451–457.

- Farley J, Rudy B (1988) Multiple types of voltage-dependent Ca^{2+} -activated K^+ channels of large conductance in rat brain synaptosomal membranes. *Biophys. J.* 53:919–934.
- Felix JA, Woodruff ML, Dirksen ER (1996) Stretch increases inositol 1,4,5-trisphosphate concentration in airway epithelial cells. *Am. J. Respir. Cell. Mol. Biol.* 14:296–301.
- Fróes MM, Correia AH, Garcia-Abreu J, Spray DC, Campos de Carvalho AC, Neto MV (1999) Gap-junctional coupling between neurons and astrocytes in primary central nervous system cultures. *Proc. Natl. Acad. Sci. USA* 96:7541–7546.
- Garaschuk O, Schneggenburger R, Schirra C, Tempia F, Konnerth A (1996) Fractional Ca^{2+} currents through somatic and dendritic glutamate receptor channels of rat hippocampal CA1 pyramidal neurons. *J. Physiol.* 491:757–772.
- Gardner-Medwin AR (1981) Possible roles of vertebrate neuroglia in potassium dynamics, spreading depression and migraine. *J. Exp. Biol.* 95:111–127.
- Gillessen T, Alzheimer C (1997) Amplification of EPSPs by low Ni^{2+} - and amiloride-sensitive Ca^{2+} channels in apical dendrites of rat CA1 pyramidal neurons. *J. Neurophysiol.* 77:1639–1643.
- Gruol DL, Jacquin T, Yool L (1991) Single channel K^+ currents recorded from the somatic and dendritic regions of cerebellar Purkinje neurons in culture. *J. Neurosci.* 11:1002–1015.
- Hablitz JJ, Heinemann U (1989) Alterations in the microenvironment during spreading depression associated with epileptiform activity in the immature neocortex. *Brain Res. Dev. Brain Res.* 46:243–252.
- Hernandez-Caceres J, Macias-Gonzalez R, Brozek G, Bures J (1987) Systemic ketamine blocks cortical spreading depression but does not delay the onset of terminal anoxic depolarization in rats. *Brain Res.* 437:360–364.
- Herreras O, Largo C, Ibarz JM, Somjen GG, Martin del Rio R (1994) Role of neuronal synchronizing mechanisms in the propagation of spreading depression in the in vivo hippocampus. *J. Neurosci.* 14:7087–7098.
- Herreras O, Somjen GG (1993) Propagation of spreading depression among dendrites and somata of the same cell population. *Brain Res.* 610:276–282.
- Hille B (1992) *Ionic Channels of Excitable Membranes* (2nd ed.). Sinauer, Sunderland, MA.
- Hodgkin AL, Huxley AF (1952) A quantitative description of membrane current and its application to conduction and excitation in nerve. *J. Physiol. (Lond.)* 117:500–544.
- Hoffman DA, Magee JC, Colbert CM, Johnston D (1997) K^+ channel regulation of signal propagation in dendrites of hippocampal pyramidal neurons. *Nature* 387:869–875.
- Holmes WR (1995) Modeling the effect of glutamate diffusion and uptake on NMDA and non-NMDA receptor saturation. *Biophys. J.* 69:734–747.
- Jakobson E (1980) Interactions of cell volume, membrane potential, and membrane transport parameters. *Am. J. Physiol.* 238:C196–C206.
- Ji S, John SA, Lu Y, Weiss JN (1998) Mechanosensitivity of the cardiac muscarinic potassium channel: A novel property conferred by the Kir3.4 subunit. *J. Biol. Chem.* 273:1324–1328.
- Jing J, Aitken PG, Somjen GG (1994) Interstitial volume changes during spreading depression in rat hippocampal slices. *Brain Res.* 604:251–259.
- Kandler K, Katz LC (1995) Relationship between dye coupling and spontaneous activity in developing ferret visual cortex. *Dev. Neurosci.* 20:59–64.
- Kavalali ET, Zhuo M, Bito H, Tsien RW (1997) Dendritic Ca^{2+} channels characterized by recordings from isolated hippocampal dendritic segments. *Neuron* 18:651–663.
- Keener J, Sneyd J (1998) *Mathematical Physiology*. Springer-Verlag, New York.
- Koch C (1998) *Biophysics of Computation*. Oxford University Press, New York.
- Koroleva VI, Vinogradova LV, Bures J (1993) Reduced incidence of cortical spreading depression in the course of pentylenetetrazol kindling in rats. *Brain Res.* 608:107–114.
- Kostyuk PG, Verchatsky (1995) *Calcium Signaling in the Nervous System*. Wiley, Chichester.
- Kraig RP, Nicholson C (1978) Extracellular ionic variations during spreading depression. *Neuroscience* 3:1045–1059.
- Lal R, Arnsdorf MF (1992) Voltage dependent gating and single channel conductance of adult mammalian atrial gap junctions. *Circ. Res.* 71:737–743.
- Largo C, Cuevas P, Somjen G, Martin del Rio R, Herreras O (1996) The effect of depressing glial function in rat brain in situ on ion homeostasis, synaptic transmission, and neuron survival. *J. Neurosci.* 16:1219–1229.
- Largo C, Ibarz JM, Herreras O (1997a) Effects of the gliotoxin fluoro-citrate on spreading depression and glial membrane potential in rat brain in situ. *J. Neurophysiol.* 78:295–307.
- Largo C, Tombaugh GC, Aitken PG, Herreras O, Somjen GG (1997b) Heptanol but not fluoroacetate prevents the propagation of spreading depression in rat hippocampal slices. *J. Neurophysiol.* 77:9–16.
- Lauritzen M, Hansen AJ (1992) The effect of glutamate receptor blockade on anoxic depolarization and cortical spreading depression. *J. Cereb. Blood Flow Metab.* 12:223–229.
- Lauritzen M, Rice ME, Okada Y, Nicholson C (1988) Quisqualate, kainate and NMDA can initiate spreading depression in the turtle cerebellum. *Brain Res.* 475:317–327.
- Leão AAP (1944a) Pial circulation and spreading depression of activity in cerebral cortex. *J. Neurophysiol.* 7:391–396.
- Leão AAP (1944b) Spreading depression of activity in the cerebral cortex. Ph.D. diss., Harvard University.
- Leão AAP (1944c) Spreading depression of activity in the cerebral cortex. *J. Neurophysiol.* 7:359–390.
- Lemieux DR, Roberge FA, Joly D (1992) Modeling the dynamic features of the electrogenic Na, K pump of cardiac cell. *J. Theor. Biol.* 154:335–358.
- Magee JC, Johnston D (1995a) Characterization of single voltage-gated Na^+ and Ca^{++} channels in apical dendrites of rat CA1 pyramidal neurons. *J. Physiol. (Lond.)* 487:67–90.
- Magee JC, Johnston D (1995b) Synaptic activation of voltage-gated channels in dendrites of hippocampal pyramidal neurons. *Science* 268:301–304.
- Mainen ZF, Sejnowski TJ (1998) Modeling active dendritic processes in pyramidal neurons. In: Koch C, Segev I, eds. *Methods in Neuronal Modeling: From Ions to Networks*. MIT Press, Cambridge, MA. pp. 171–210.
- Marrannes R, Willems R, De Prins E, Wauquier A (1998) Evidence for a role of the N-methyl-D-aspartate (NMDA) receptor in cortical spreading depression in the rat. *Brain Res.* 457:226–240.
- Martins-Ferreira H, Ribeiro LJ (1995) Biphasic effects of gap junctional uncoupling agents on the propagation of retinal spreading depression. *Braz. J. Med. Biol. Res.* 28:991–994.

- Mayer ML, Westbrook GL (1987) Permeation and block of n-methyl-D-aspartic acid receptor channels by divalent cations in mouse cultured central neurons. *J. Physiol.* 394:501–527.
- McCown TJ, Breese GR (1990) Effects of apamin and nicotinic acetylcholine receptor antagonists on inferior collicular seizures. *Eur. J. Pharmacol.* 187:49–58.
- McLachlan RS (1992) Suppression of spreading depression of Leao in neocortex by an N-methyl-D-aspartate receptor antagonist. *Can. J. Neurol. Sci.* 19:487–491.
- Mienville JM, Barker JL, Lange GD (1996) Mechanosensitive properties of BK channels from embryonic rat neuroepithelium. *J. Membrane Biol.* 153:211–216.
- Morton KW, Mayers KF (1994) *Numerical Solution of Partial Differential Equations: An Introduction*. Cambridge University Press, Cambridge.
- Müller M, Somjen GG (1998) Inhibition of major cationic inward currents prevents spreading depression-like hypoxic depolarization in rat hippocampal tissue slices. *Brain Res.* 812:1–13.
- Nadarajah B, Parnavelas JG (1999) Gap junction-mediated communication in the developing and adult cerebral cortex. *Novartis Found. Symp.* 219:157–174.
- Nedergaard M, Cooper AJ, Goldman SA (1995) Gap junctions are required for the propagation of spreading depression. *J. Neurobiol.* 28:433–444.
- Nellgard B, Wieloch T (1992) NMDA-receptor blockers but not NBQX, an AMPA-receptor antagonist, inhibit spreading depression in the rat brain. *Acta Physiol. Scand.* 146:497–503.
- Nicholson S, Syková E (1998) Extracellular space structure revealed by diffusion analysis. *Trends Neurosci.* 21:207–215.
- Noma A, Tsuboi N (1987) Dependence of junctional conductance on proton, calcium and magnesium ions in cardiac paired cells of guinea pig. *J. Physiol.* 382:193–211.
- Peinado A, Yuste R, Katz LC (1993) Gap junctional communication and the development of local circuits in neocortex. *Cereb. Cortex* 3:488–498.
- Pleumsamran A, Kim D (1995) Membrane stretch augments the cardiac muscarinic K⁺ channel activity. *J. Membr. Biol.* 148:287–297.
- Psarropoulou C, Avoli M (1993) 4-Aminopyridine-induced spreading depression episodes in immature hippocampus: Developmental and pharmacological characteristics. *Neuroscience* 55:57–68.
- Qian N, Sejnowski TJ (1989) An electro-diffusion model for computing membrane potentials and ionic concentrations in branching dendrites, spines and axons. *Biol. Cybern.* 62:1–15.
- Reggia JA, Montgomery D (1996) A computational model of visual hallucinations in migraine. *Comput. Biol. Med.* 26:133–141.
- Reinhart PH, Chung S, Levitan IB (1989) A family of calcium-dependent potassium channels from rat brain. *Neuron* 2:1031–1041.
- Revetz K, Ruppin E, Goodall S, Reggia JA (1998) Spreading depression in focal ischemia: A computational study. *J. Cereb. Blood Flow Metab.* 18:998–1007.
- Rörig B, Klaus G, Sutor B (1995) Dye coupling between pyramidal neurons in developing rat prefrontal and frontal cortex is reduced by protein kinase A activation and dopamine. *J. Neurosci.* 15:386–400.
- Rusakov DA, Kullmann DM (1998) Geometric and viscous components of the tortuosity of the extracellular space in the brain. *Proc. Natl. Acad. Sci. USA* 95:8975–8980.
- Sah P (1996) Ca²⁺-activated K⁺ currents in neurones: Types, physiological roles and modulation. *TINS* 19:150–154.
- Sasaki N, Mitsuiye T, Noma A (1992) Effects of mechanical stretch on membrane currents of single ventricular myocytes of guinea pig hearts. *Jap. J. of Physiol.* 42:957–970.
- Scheller D, Tegtmeier F, Schlue WR (1998) Dose-dependent effects of tetraethylammonium on circling spreading depressions in chicken retina. *J. Neurosci. Res.* 51:85–89.
- Schneggenburger R (1996) Simultaneous measurement of Ca⁺⁺ influx and reversal potentials in recombinant n-methyl-D-aspartate receptor channels. *Biophys. J.* 70:2165–2174.
- Shapiro BE (2000) An electrophysiological model of gap-junction mediated cortical spreading depression including osmotic volume changes. Ph.D. diss., University of California, Los Angeles.
- Simbürger E, Stang A, Kremer M, Dermietzel R (1997) Expression of connexin43 mRNA in adult rodent brain. *Histochem. Cell. Biol.* 107:127–137.
- Sloper JJ, Powell TP (1978) Gap junctions between dendrites and somata of neurons in the primate sensori-motor cortex. *Proc. R. Soc. Lond. B. Biol. Sci.* 203:39–47.
- Somjen GG, Aitken PG, Czeh GL, Herreras O, Jing J, Young JN (1992) Mechanism of spreading depression: A review of recent findings and a hypothesis. *Can. J. Physiol. Pharmacol.* 70:S248–S254.
- Stuart G, Sakmann, B (1994) Active propagation of somatic action potentials into neocortical pyramidal cell dendrites. *Nature* 367:69–72.
- Tas, PWI, Massa PT, Koschel K (1986) Preliminary characterization of an Na⁺, K⁺, Cl⁻-co-transport activity in cultured human astrocytes. *Neurosci. Lett.* 70:369–377.
- Tas PWI, Massa PT, Kress HG, Koschel K (1987) Characterization of a Na⁺, K⁺, Cl⁻-contransport in primary cultures of rat astrocytes. *Biochim. Biophys. Acta* 903:411–416.
- Traub RD, Jefferys JGR, Miles R, Whittington M, Toth K (1994) A branching dendritic model of a rodent CA3 pyramidal neurone. *J. Physiol. (Lond.)* 481:79–95.
- Tuckwell HC (1980) Predictions and properties of a model of potassium and calcium ion movements during spreading depression. *Intern. J. Neurosci.* 10:145–164.
- Tuckwell HC (1981) Simplified reaction-diffusion equations for potassium and calcium ion concentrations during spreading cortical depression. *Intern. J. Neurosci.* 12:95–107.
- Tuckwell HC, Hermansen CL (1981) Ion and transmitter movements during spreading cortical depression. *Intern. J. Neurosci.* 12:109–135.
- Tuckwell HC, Miura RM (1978) A mathematical model for spreading depression. *Biophys. J.* 23:257–276.
- Tuttle R, Masuko S, Nakajima Y (1986) Freeze-fracture study of the large myelinated club ending synapse on the goldfish Mauthner cell: Special reference to the quantitative analysis of gap junctions. *J. Comp. Neurol.* 246:202–211.
- van der Want JJJ, Gramsbergen A, Ijkema-Paassen J, de Weerd H, Liem RSB (1998) Dendro-dendritic connections between motoneurons in the rat spinal cord: An electron microscopic investigation. *Brain Res.* 779:342–345.
- Van Harreveld A (1984) The nature of the chick's magnesium-sensitive retinal spreading depression. *J. Neurobiol.* 15:333–343.
- Vergara C, Latorre R, Marrion NV, Adelman JP (1998) Calcium-activated potassium channels. *Curr. Opin. Neurobiol.* 8:321–329.

Vogel R, Weingart R (1998) Mathematical model of vertebrate gap junctions derived from electrical measurements on homotypic and heterotypic channels. *J. Physiol.* 510:177–189.

Yamada WM, Koch C, Adams PR (1998) Multiple channels and calcium dynamics. In: Koch C, Segev I, eds. *Methods in Neuronal Modeling: From Ions to Networks*. MIT Press, Cambridge, MA. pp. 137–170.